Hindawi
Geofluids
Volume 2019, Article ID 1280721, 23 pages
https://doi.org/10.1155/2019/1280721

Research Article

Fault "Corrosion" by Fluid Injection: A Potential Cause of the November 2017 M_W 5.5 Korean Earthquake

Rob Westaway and Neil M. Burnside

James Watt School of Engineering, University of Glasgow, Glasgow G12 8QQ, UK

Correspondence should be addressed to Rob Westaway; robert.westaway@gla.ac.uk

Received 10 January 2019; Revised 16 April 2019; Accepted 8 June 2019; Published 24 July 2019

Guest Editor: Victor Vilarrasa

The November 2017 M_W 5.5 Pohang earthquake is one of the largest and most damaging seismic events to have occurred in the Korean peninsula over the last century. Its close proximity to an Enhanced Geothermal System (EGS) site, where hydraulic injection into granite had taken place over the previous two years, has raised the possibility that it was anthropogenic; if so, it was by far the largest earthquake caused by any EGS project worldwide. However, a potential argument that this earthquake was independent of anthropogenic activity considers the delay of two or three months before its occurrence, following the most recent injection into each of the wells. A better understanding of the physical and chemical processes that occur following fluid injection into granite is thus warranted. We show that hydrochemical changes occurring while surface water, injected into granite, reequilibrates chemically with its subsurface environment, can account for time delays for earthquake occurrence of such duration, provided the seismogenic fault was already critically stressed, or very close to the condition for slip. This candidate causal mechanism counters the potential argument that the time delay militates against an anthropogenic cause of the Pohang earthquake and can account for its relatively large magnitude as a consequence of a relatively small-volume injection. The resulting analysis places bounds on combinations of physical and chemical properties of rocks, injected volume, and potential postinjection time delays for significant anthropogenic seismicity during future EGS projects in granite.

1. Introduction

Anthropogenic seismicity associated with geoengineering projects is emerging as a significant issue for society. Engagement between project developers and the public requires transparent discussion of risks, which means dealing with low-probability adverse consequences, including consequences of "unknown unknowns" affecting geomechanical processes (e.g., [1–3]). Until recently, no deaths or injuries had been attributed to any anthropogenic earthquake caused by fluid injection [3]. The Newcastle, Australia, earthquake of 27 December 1989 (M_W 5.6) resulted in 13 fatalities and ~£3 billion worth of damage but was caused by coal mining, not fluid injection (e.g., [4]). Nonetheless, the magnitude (M_W) 5.5 earthquake that occurred at Pohang, South Korea, on 15 November 2017, which injured 135 people, displaced >1700 people into emergency accommodation, and caused >US$75M in damage to >57,000 structures along with >US$300M of total economic impact (e.g., [5]), was tentatively linked at an early stage to injection activity for a nearby EGS project (e.g., [6, 7]), focusing attention on this topic. However, potential reasons why this earthquake might be considered unrelated to the EGS project include, first, the time delay of 2-3 months since the most recent injection at the site (e.g., [8]). The second reason is the large size (magnitude, M_W, or seismic moment, M_O) of the earthquake in comparison with the relatively small volume V of fluid injected (e.g., [6, 7]), given existing theory for predicting the upper bound to M_W or M_O as a function of V [9]. Nonetheless, an official report, commissioned by the Republic of Korea government, released in March 2019, has asserted that the injection activity at this EGS site did indeed cause the 15 November 2017 earthquake [5, 10], the proposed causal mechanism being poroelasticity, thus

depending on the combination of injected volume and the pressure at which it was injected, rather than just the injected volume.

The Pohang EGS project is located ~6 km north of the centre of the industrial city of Pohang and ~3 km east of the town of Heunghae (Figure 1). Two deep wells have been drilled, reaching ~4.3 km depth in Permian granite (Table 1); one (PX-2) vertical and the other (PX-1) also initially drilled vertically, subsequently side-tracked to a WNW deviation by ~600 m (Figure 2), the bottom hole depths (below sea-level) being 4189 m for well PX-1 and 4314 m for well PX-2 [5]. Magnetotelluric exploration early in the project revealed a zone of high electrical conductivity, interpreted as a water-bearing fault, dipping steeply NW [11, 12]. However, subsequent investigations (e.g., [13, 14]) led to revision of the developers' conceptual model which, in its final form, envisaged utilization for fluid circulation of a WNW-ESE fracture [15], thus not incorporating the previously identified NW-dipping fault into the project design. A significant loss of circulation of drilling fluid was noted at 3434 m depth during the initial (vertical) drilling of well PX-1, indicating that a permeable fault or fracture had been crossed [16]. An even greater loss of circulation was reported, concentrated between depths of 3816 and 3840 m, during drilling of well PX-2, directly beneath a zone of fault gouge spanning 3790-3816 m [5] (Figure 3). These observations indicate that a major fault was transected [5] (cf. Figure 4). The latter loss of circulation (amounting to ~650 m^3) in November 2015 was followed by a "burst" of microearthquakes lasting roughly for a month [5], indicating that this major fault, or other faults hydraulically connected to it, was already critically stressed. However, this fault intersection was subsequently sealed by casing the wellbore. Injection experiments, to attempt to stimulate the geothermal reservoir, using hydraulic fracturing or "hydroshearing" to improve its hydraulic properties, took place in well PX-1 in December 2016 and in August 2017 and in well PX-2 in February 2016, April 2017, and September 2017 (e.g., [7]); the overall volume injected into both wells has been ~12,000 m^3, with ~7000 m^3 of flowback [5, 17].

The "cloud" of aftershocks that followed the Pohang mainshock (Figure 2) reveals a NW-dipping fault plane in the same place (given the uncertainties in the studies) as the fault recognized in the preliminary exploration [11, 12]; to facilitate discussion, we designate this hitherto unnamed structure as the Namsong Fault, named after a nearby village (located at 36.100°N, 129.368°E, ~1 km SW of the drilling site; Figure 1). As shown in Figure 2, the fault plane delineated by these aftershock locations projects across the wellbore at ~3800 m depth, consistent with the reported fault gouge and loss of circulation in well PX-2 [5] (Figure 3). The Pohang mainshock involved reverse slip with a component of right-lateral slip [6, 7] (Table 2 and Figure 5). The ~4 cm maximum coseismic uplift of the Earth's surface, revealed by satellite radar imaging, confirms the geometry of the fault [6]. Logging tools inserted into well PX-2 in August 2018 could not reach below 3783 m depth [5], suggesting that this well had been sheared by the coseismic slip in November 2017 on the fault depicted in Figure 3. The Namsong Fault,

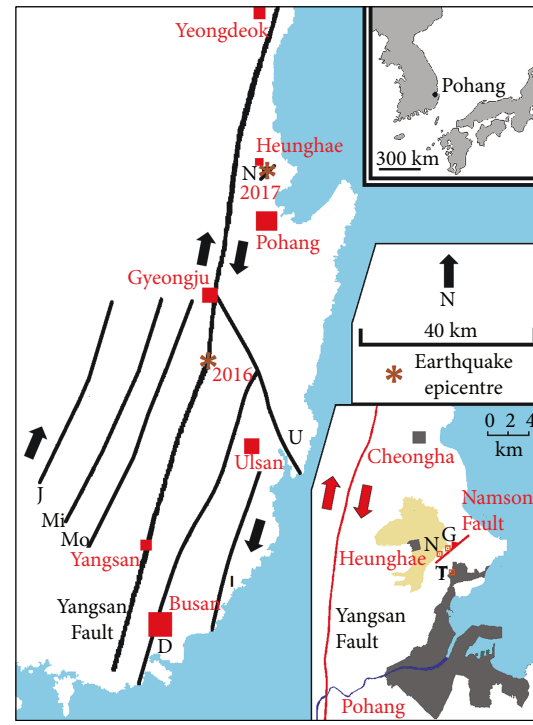

Figure 1: Location map for the city of Pohang in the SE part of the Korean peninsula (upper inset showing wider location, lower inset showing greater local detail), showing Late Cenozoic right-lateral faults (from [96]), the Namsong Fault (from [7]), and the epicentres of the 12 September 2016 and 15 November 2017 earthquakes (from [7, 46]). The right-lateral faults depicted follow prominent fault-line escarpments that dominate the local topography, being readily visible on topographic maps and satellite imagery (such as Figure 1 of [96]). The local inset shows the Namsong Fault (depicted schematically at the updip limit of coseismic reactivation in 2017, from [6]), the Heunghae alluvial plain (pale shading), the EGS project site (G), Namsong village (N), and the Pohang thermal spa resort that yielded hydrochemical data (T; coordinates from [97]).

thus reactivated, has no mapped surface trace and was unrecognized (except for the initial tentative interpretation [11, 12] of the magnetotelluric evidence, which did not inform the ultimate design of the EGS project) before the November 2017 earthquake. Although the evidence now available reveals it to be a major structure [5] (Figure 3), it remains unclear whether it is confined to the Pohang granite or continues upward into any of the overlying stratigraphy (Table 1) (cf. [18]).

The standard procedure [19] for assessing whether an earthquake is anthropogenic considers spatial proximity and temporal correlation with fluid injection, and geomechanical calculations indicating that the injection could have caused the seismogenic fault to slip, the latter typically relating shear and normal stresses and fluid pressure to the standard Coulomb failure criterion. For the Pohang mainshock, spatial proximity is obvious (Figure 2). The fluid pressure reached very high values during the first injection experiment in well PX-2 in February 2016 (maximum wellhead pressure 89 MPa causing bottom-hole pressure 132 MPa at 4368 m depth [15]), exceeding the estimated minimum principal stress

Table 1: Pohang borehole stratigraphy.

Lithology	Name	Depth (m)	Age	Note
Mudstone	Yeonil group	0	Middle Miocene	1
Tuff	Beomgokri group	206	21.7 ± 1.2 Ma	2
Mudstone	Yucheon group	330	66.8 ± 0.7 Ma	3
Andesite	Gyeongsang volcanics	1250	Late Cretaceous	4
Granodiorite	Pohang granite	2356	262.4 ± 3.6 Ma	5

Data for well PX-1 are from [13, 16], supplemented here with additional information. Depth is to the top of each stratigraphic division. Notes: 1: biostratigraphic age from [93]. 2: youngest $^{206}Pb/^{238}U$ date reported on detrital zircon, from [36], in overlying mudstone. Name from [41]. 3: lacustrine mudstone with interbedded sandstone, tuff, and rhyolitic lava. Representative $^{206}Pb/^{238}U$ date on zircon, from [36], for the rhyolite. Nomenclature from [32, 94]. 4: interbeds of andesite and andesitic tuff. Nomenclature from [32]. 5: granodiorite with gabbroic dykes. Oldest $^{206}Pb/^{238}U$ date on zircon, from [36].

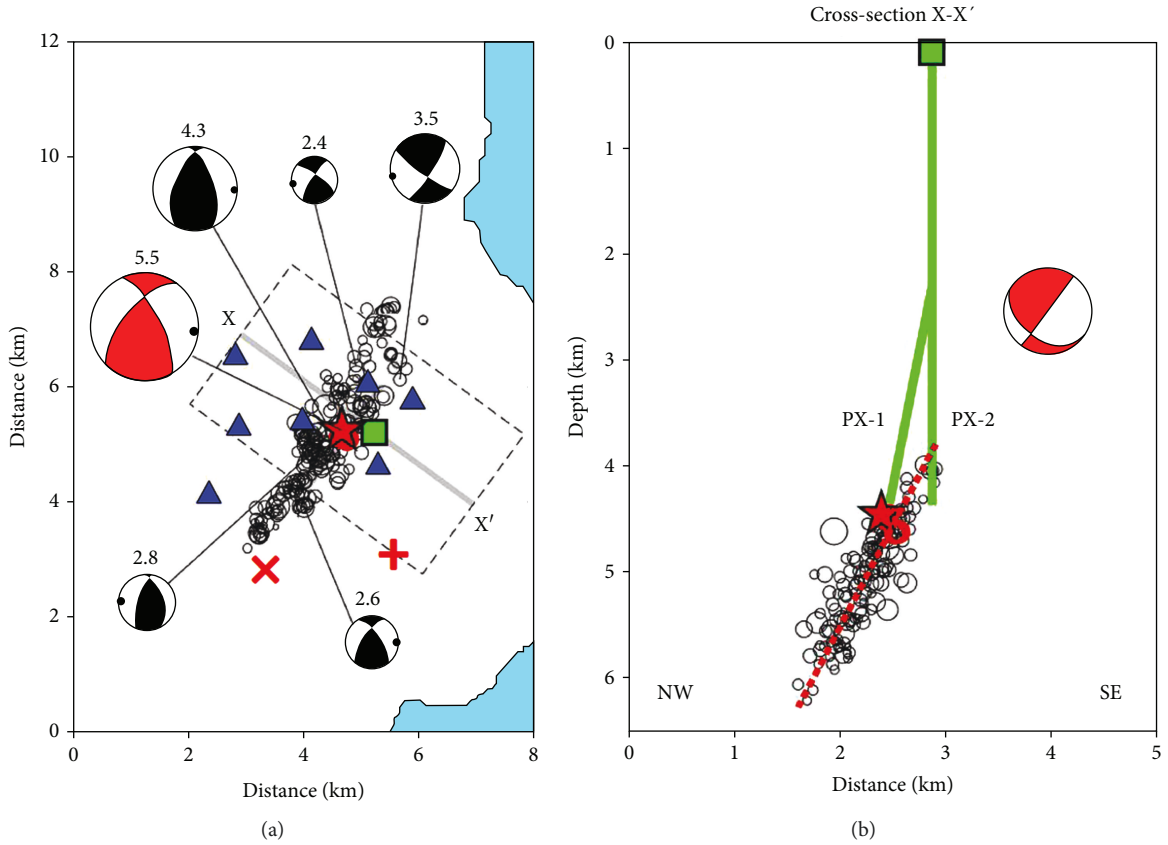

Figure 2: Locations of earthquakes at Pohang in November 2017: foreshocks (red circles), the 15 November mainshock (red star), and aftershocks (black circles). Also shown are stations of the local seismograph network (blue triangles), the EGS site (green square), the thermal spa resort (red + symbol; coordinates from [97]), and the borehole that yielded the in situ stress measurements discussed by [58] (red × symbol). Focal mechanisms of the mainshock and five principal aftershocks, each labelled by M_W, are drawn as standard lower (or back) focal hemisphere projections with compressional quadrants shaded. Modified from [7]. (a) map. (b) NW-SE cross-section along line illustrated in (a), showing schematically the two deep wells (solid green lines) and the interpreted plane of the Namsong Fault (dashed red line).

at depth [15]; had this pressure been transmitted directly to the Namsong Fault (i.e., had the fluid pressure acting on this fault risen to 132 MPa or any similar value), it would have slipped during this injection (see below). Regarding any temporal association, full details of the subsequent injection experiments have not been reported by the developers; however, the published summary [7] includes injection in well PX-1 in August 2017 and in well PX-2 in September 2017, respectively, three and two months before the mainshock. Although physical mechanisms are known that can cause seismicity delayed following fluid injection (e.g., [20, 21]), none has hitherto explained a delay as long as 2-3 months.

One potential candidate mechanism, poroelastic diffusion of stress, has been proposed as the cause of "natural" seismicity with delays of months following climatic triggering (e.g., [22]). Many case studies of seismicity associated

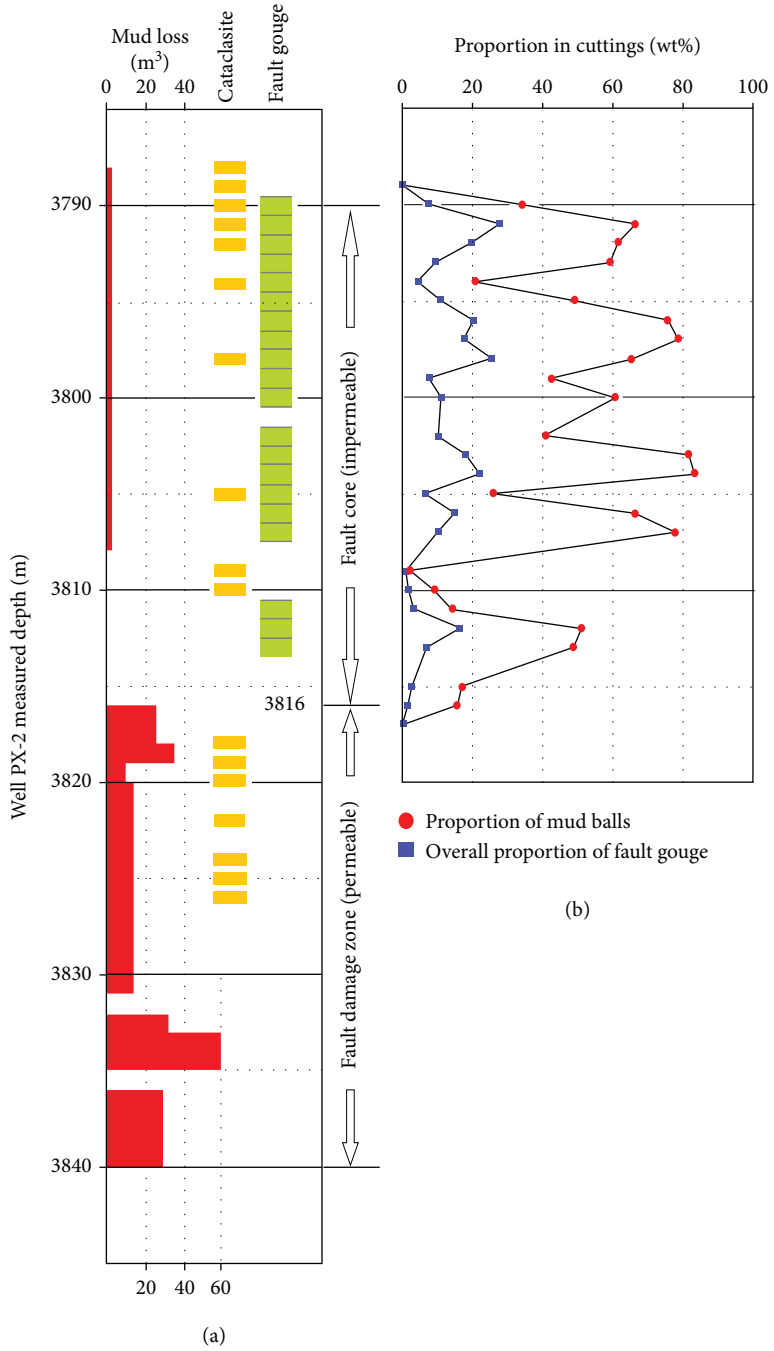

Figure 3: Enlargement of the intersection in Figure 2(b) between well PX-2 and the Namsong Fault, showing (a) reports of fault gouge, cataclasite, and loss of drilling mud, from drilling logs, and (b) proportions of fault gouge from subsequent laboratory analysis of cuttings. Modified from Figure O-3(e) of [5]. Many of the larger (centimetre-sized) cuttings from this depth range were "mud balls" containing large proportions of fault gouge and cataclasite; [5] provides further details. Interpretation of impermeable fault core and permeable fault damage zone, after [86, 87].

with fluid injection or extraction have indeed been explained as poroelastic effects (e.g., [23–27]). Poroelastic modelling of the flow rate/pressure dataset for the August 2017 stimulation has been reported [17, 28]. However, this work is subject to significant limitations, first, because its analysis is two-dimensional (2-D), assuming cylindrical symmetry, with the injected fluid assumed to flow radially outward and not upward or downward. Second, it assumes that the flow is governed by matrix permeability and not fracture permeability, let alone permeability created by the development of new fractures as the injection proceeds. Such 2-D modelling has no way of incorporating any interaction between the injected fluid and the Namsong Fault; three-dimensional modelling is evidently desirable but is beyond the scope of the present

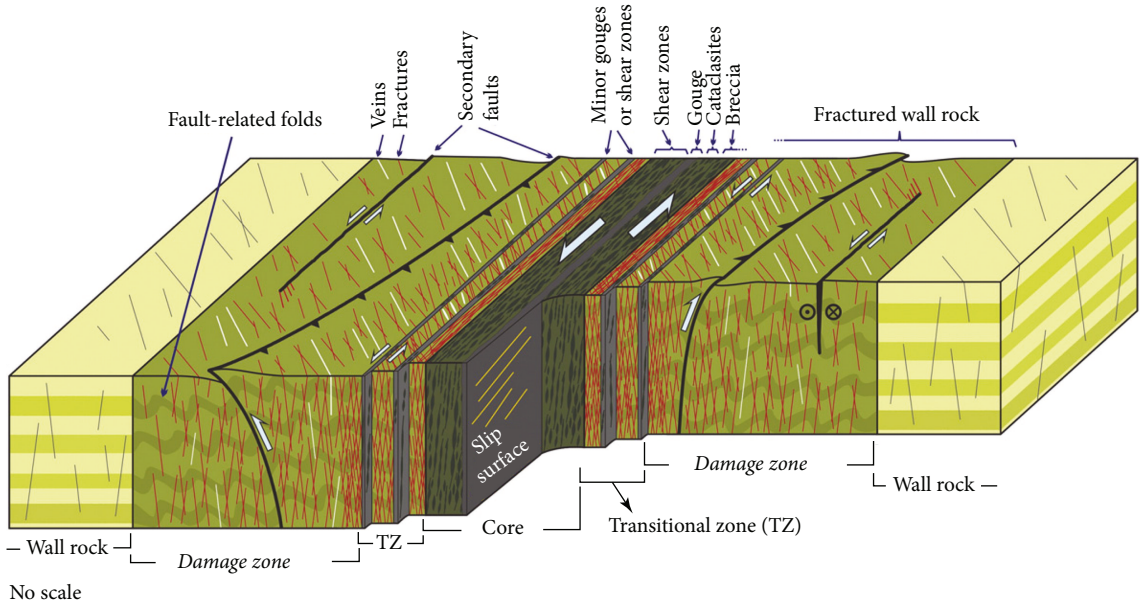

Figure 4: Conceptual block-diagram illustrating the complexity of a major fault, from Figure 1 of [88]. This diagram shows the main components of a fault zone (i.e., the fault core and damage zones) and structural elements and features in each component, for comparison with Figure 3. A transitional (or mixed) zone is depicted at the boundary between the impermeable fault core and permeable damage zones. Fracture development into such a fault zone by hydroshearing might interact with permeable elements, including fractures and secondary faults within the damage zone and shear zones within the transitional zones.

Table 2: Earthquake source parameters.

Source	M_W	M_O (10^{17} Nm)	Fault plane			*P*-axis		*T*-axis	
			ϕ (°)	δ (°)	λ (°)	θ (°)	α (°)	θ (°)	α (°)
U.S. Geological Survey [95]	5.5	2.01	203	45	108	1	101	78	105
Kim et al. [7]	5.4	ND	216	65	150	1	268	38	177
Grigoli et al. [6]	5.5	1.73	221	66	130	12	283	51	178
Lee et al. [5]	5.56	2.45	214	43	141	12	090	55	198

Focal mechanism determinations for the Pohang mainshock. Symbols denote: ϕ, strike; δ, dip; λ, rake; θ, plunge; and α, azimuth; ND indicates "not determined"; M_W and M_O denote moment magnitude and seismic moment.

study. Nonetheless, hypocentral locations of the microearthquakes that accompanied this injection experiment indicate downward propagation below the ~4.2 km deep PX-1 injection point to a depth of ~4.4 km [17], the deepest adjoining the projection of the Namsong Fault below the injection point, especially if the dip of the fault is as low as 43° (Table 1) (cf. Figure 2). The lack of any deeper propagation suggests that the injected fluid interacted with this fault.

As was noted above, poroelasticity has also been proposed as the cause of the 15 November 2017 Pohang earthquake [5], the modelling for this report treating the Pohang granite as a material of uniform (0.01 m^2 s^{-1}) hydraulic diffusivity, with a lower diffusivity for the Namsong Fault core and a higher diffusivity for the adjoining damage zone (cf. Figure 3), thus—again—not explicitly incorporating the anticipated fractured nature of these fault rocks (cf. Figure 4). This modelling did not investigate injection into well PX-1, but determined that the injection experiments in well PX-2 increased the fluid pressure on the Namsong Fault by ~0.1 MPa in April 2017 and by ~0.08 MPa by 15 November 2017, the latter change being the cause of the M_W 5.5 earthquake [5]. However, realistic calculations of poroelastic stress changes for a fractured material as complex as the Pohang granite (cf. Figure 6), as a consequence of fluid injection under a state of triaxial stress, would be extremely difficult and are beyond the scope of the present study. Nonetheless, the fact that the above-mentioned calculations predict a smaller poroelastic pressure increase at the Namsong Fault in November 2017 compared with at times beforehand means that the analysis (from [5]) does not in fact account for the timing of the 15 November 2017 earthquake. In addition, considerations of proximity between the two wells and the Namsong Fault indicate the potential importance of injection into well PX-1: top of the open-hole section of well PX-2 is ~400 m below the Namsong Fault, whereas if this fault dips at only 43° [5], it passes barely 100 m below the bottom of well PX-1, the aforementioned limited downward propagation of the seismicity accompanying this injection [17] thus suggesting that the injected fluid, and the fracture network it created, reached this fault. Such considerations raise the possibility that significant causal factors of the 15 November 2017 Pohang earthquake have been overlooked in the work reported so far, including [5].

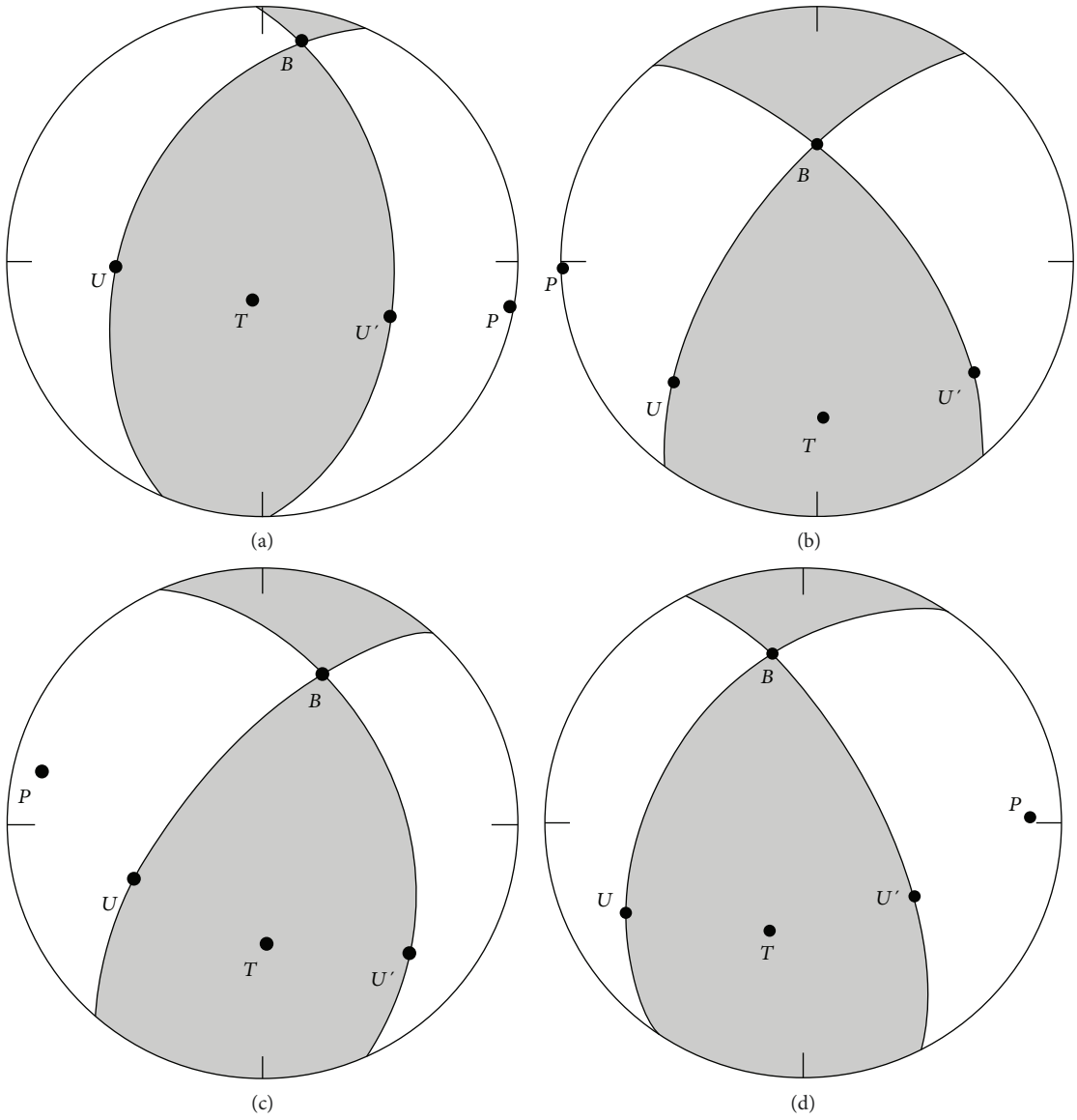

Figure 5: Four determinations of the focal mechanism of the Pohang mainshock. Diagrams are displayed as standard equal area projections of the lower focal hemisphere, with north at the top and compressional quadrants of the double-couple P-wave radiation pattern shaded. P, T, and B denote the P-axis, T-axis, and null axis, respectively; U denotes the slip vector, and U' denotes the direction perpendicular to the fault plane. (a) Determined by the U.S. Geological Survey [95]; (b) determined by Kim et al. [7]; (c) determined by Grigoli et al. [6]; (d) determined by Lee et al. [5].

Guided in part by the above considerations, we investigate another potential candidate mechanism for seismicity, the effect of injected surface water, reacting with the granite adjoining the fault, on the local state of stress. Such an effect can be inferred from studies of the alteration history of granite intrusions, which demonstrate precipitation of quartz within faults or fractures at temperatures of ~150°C (e.g., [29]), thus demonstrating interaction between solid and dissolved phases under such conditions. This interaction is shown to be able to account for induced seismicity with delays of this order. Anthropogenic earthquakes with longer delays are known; for instance, the magnitude 2.7 event of 15 August 2009 at Landau, Germany, occurred two years after hydraulic stimulation of granite [30], although no causal mechanism has hitherto been suggested that can account for this delay. The seismicity following the injection in 2006 into granite beneath the Swiss city of Basel included an event of magnitude 3.2 with a delay of two months, followed by smaller events spanning more than a year [31]. The proposed mechanism might be applicable to other instances such as these; hitherto, analyses of induced seismicity following injection into granite have typically not considered groundwater hydrochemistry, and appropriate hydrochemical data from geothermal projects have typically been unavailable.

Our analysis will focus on the August 2017 stimulation of well PX-1 as this is the best-documented hydrochemically of the Pohang injection experiments. However, this does not mean that we regard this injection as the sole cause of the

Figure 6: Outcrop of Yeongdeok granite near Jipum (36.4478351°N, 129.2705272°E; near the town of Yeongdeok, ~50 km north of Pohang; Figure 1), showing its highly fractured character. Tape measure (diameter ~8 cm) provides scale. This granite is petrologically similar to the Pohang granite and part of the same Permian magmatic suite (e.g., [37]). Its highly fractured character can be considered indicative of the physical state of the Pohang granite. For the Yeongdeok granite, the typical spacing of fractures has been measured as ≤0.3 m [98]. However, many of these fractures will have been formed during the last ~1 km of erosional unloading (cf. [99]); we thus adopt a nominal fracture spacing of 0.5 m for our analysis of the Pohang granite.

M_W 5.5 earthquake; multiple injection experiments, plus the aforementioned release of drilling fluid, might well have contributed to the hydrochemical "corrosion" of the Namsong Fault, but the information available on these activities is incomplete. We shall first summarize background information on the Pohang site, including on its thermal state and state of stress. We then describe the process of collecting and analyzing water samples from this site. Finally, we analyze the geomechanics of the site, including calculations of the effect of hydrochemical "corrosion" on the state of stress.

2. Conditions at the Pohang EGS Site

The Korean peninsula has experienced a complex tectonic history, with multiple phases of crustal deformation contributing to the stratigraphy evident in the Pohang boreholes (Table 1). Details differ between accounts (e.g., [32–35]), and some aspects remain subject to considerable uncertainty. Nonetheless, to summarize a complex story, granite intrusion during the Permian is attributed to subduction during the suturing together of previously separated continental crustal provinces, now merged within Korea. This phase of tectonic activity created the Pohang granite and neighbouring intrusions, which are reliably dated (e.g., [36, 37]). Subsequent phases of crustal deformation during the Mesozoic reflect the changing geometry of subduction, beneath the eastern margin of Asia, of oceanic plates within the Pacific basin. Thus, for example, during much of the Cretaceous, oblique subduction of the Izanagi Plate was accompanied by island arc volcanism and the development of the terrestrial Gyeongsang backarc basin in SE Korea (e.g., [32]). The Pohang granite, unroofed by this time, was reburied beneath sediments and volcanic rocks (Table 1). Also, during the Cretaceous, pervasive granitic magmatism and regional hydrothermal mineralization were consequences of low-angle subduction of relatively young, hot, oceanic lithosphere that had formed at the oceanic spreading centre between the Izanagi and Pacific plates (e.g., [38, 39]).

The most recent tectonic processes affecting the Pohang area relate to the Miocene crustal extension and oceanic spreading in the Sea of Japan backarc basin (e.g., [40]) to the east of Korea. Faulting associated with this extension passes onshore into SE Korea, continuing southward through

the Pohang area as the NNE-SSW-oriented right-lateral Yangsan Fault (e.g., [33, 41, 42]; Figure 1). The Yangsan Fault has slipped tens of kilometres (~35 km according to [33]; ~50 km according to [43]), displacing the contacts between zones of Cretaceous mineralization (e.g., [40]). A relatively complex fault pattern is thus evident in the Pohang area at this rightward step in right-lateral faulting (e.g., [33, 41, 42]). Right-lateral slip on the Yangsan Fault continues to the present day, evidenced by palaeoseismic studies (e.g., [44]), historical earthquakes (e.g., [45]), and instrumentally recorded events. The Gyeongju earthquake (M_W 5.5) of 12 September 2016, which occurred ~40 km SSW of the Pohang EGS site (e.g., [46]; Figure 1), demonstrates that this fault remains active. Using kinematic indicators on exposures of Quaternary faults, Park et al. [47] determined the state of stress for the Pohang area with maximum principal stress plunging at 8° towards an azimuth of 250°, intermediate principal stress plunging at 7° towards 159°, and minimum principal stress plunging at 79° towards 059°. However, no evidence of Quaternary slip on the Namsong Fault has previously been reported; the age of its most recent slip (before 15 November 2017) is unknown.

At the time of the August 2017 injection, well PX-1 was cased, with internal and external diameters of 6" and 7", to a measured depth (MD) of 4069 m (4049 m below sea level), with a 313 m open-hole section of diameter 8.5" in the Pohang granite to 4382 m MD. This open-hole section is at true vertical depth (TVD) between 3940 and 4237 m. For comparison, well PX-2 is vertical, with its open-hole section between 4228 and 4368 m TVD. The August 2017 injection experiment was intended to test a "soft" stimulation concept, involving cyclic variations in an injection rate, with the aim of mitigating induced seismicity, causing very small microearthquakes by shearing preexisting fractures to hopefully increase permeability and thus hydraulically connect the two wells [48]. In these circumstances, whether shearing of preexisting fractures propagates upward or downward depends on whether the vertical stress gradient exceeds the vertical fluid pressure gradient (e.g., [49, 50]). The magnitude and orientation of the stress tensor at Pohang are not known with confidence ([15]; see below); focal mechanisms of the "nanoearthquakes" that accompanied the injection experiments have not been reported. Nonetheless, as already noted, the hypocentres of the events that accompanied the August 2017 injection experiment propagated downward below the ~4.2 km deep PX-1 injection point to the Namsong Fault around ~4.4 km depth [17], suggesting that the "hydroshearing" caused by this injection reached this fault.

2.1. Thermal State. The Pohang EGS project was designed assuming a nominal bottom-hole temperature (BHT) of 180°C [51], for a nominal 5 km depth [52], but measurements of the undisturbed BHT in wells PX-1 and PX-2 were not made by the developers. Nonetheless, a 103°C temperature has been reported [16] at 2250 m depth, just above the top of the Pohang granite at 2356 m [16]. The surface heat flow is 94 mW m^{-2} in a nearby borehole [53]; given the 28°C km^{-1} geothermal gradient in the granite [53], a temperature of ~160°C can be estimated at ~4.3 km depth (i.e., 103°C + (~4.3-~2.4 km) × 28°C km^{-1} = ~160°C).

The initial temperature of the injected water reflects its surface environment, being up to ~30°C for the injection into well PX-1 in August 2017 (see below, also the supplementary file available here)). On entering any fracture of width W, this water thus experienced postinjection warming by up to ~130°C, making it important to estimate the timescale for this warming as this will affect rates of hydrochemical reaction. We have made an approximate assessment of the required timescale using analytic theory (equation (3) on page 54 of [54]). For a temperature difference of ~130°C, the time required for a temperature rise to within ~1°C of the initial temperature of the surroundings to the fracture can thus be determined as ~1000 × W^2/κ, where κ is the thermal diffusivity of water (~0.14 mm^2 s^{-1}). This timescale thus ranges from ~2 hours for W = 1 mm to ~10 days for W = 10 mm and ~3 years for W = 100 mm. These estimated timescales for warming of injected water bear upon the analysis of the geomechanics (see below).

2.2. State of Stress. The maximum principal stress beneath Korea is roughly east-west, caused by the convergent plate motions across the western margin of the Pacific basin (e.g., [55]). However, the orientations of the minimum and intermediate principal stresses show considerable variability within Korea (e.g., [55–57]). The EGS project developers estimated the stress field at a representative depth of 4278 m; their arguments are set out in their publications (e.g., [15]). They thus deduced a lithostatic vertical principal stress σ_V at this depth of 110 MPa, a horizontal maximum principal stress σ_H in the range 116-139 MPa, and a horizontal minimum principal stress σ_h in the range 82-105 MPa. A wide range of uncertainty, between N65°E and S50°E (or 065-130°), was estimated for the azimuth of σ_H, reflecting uncertainty in the analysis, which nonetheless indicates $\sigma_h < \sigma_V < \sigma_H$. This analysis extrapolated in situ stress measurements made in shallower boreholes to greater depths; the data include the σ_H azimuth (with the intermediate principal stress vertical) of 135 ± 3° (S45 ± 3°E) at ~700 m depth from hydraulic fractures and 136 ± 4° (S44 ± 4°E) at ~800 m depth from drilling-induced fractures [58], these measurements being made in Early Miocene tuff (Table 1) in a borehole ~4 km SW of the Pohang EGS site. However, other case studies indicate that such extrapolation cannot be done with confidence, as the stress tensor orientation may change significantly with depth (especially between contrasting lithologies) (e.g., [21, 59]), a phenomenon recognized in Korea [57]. For example, Chang et al. [56] reported a typical WSW-ENE maximum principal stress and a typical vertical minimum principal stress in SE Korea from measurements in shallow (depth <350 m) boreholes. The analysis by Kim et al. [58] is also inconsistent with other work (e.g., [55, 60]) which indicates reverse-faulting focal mechanisms in the region, also consistent with a vertical minimum principal stress (although strike-slip earthquakes have also been reported). It also contrasts with the determination, already noted, of a near-vertical minimum principal stress in the Pohang area

from kinematic indicators on faults [47]. These inconsistencies indicate that the stress field in the Pohang area is subject to some uncertainty.

Three dimensional geomechanics case studies such as this can in principle be analyzed trigonometrically (e.g., [61, 62]). However, we have instead used a vector geometry approach [21] as this produces equivalent results with simpler calculations. Searching through the combinations of magnitudes and orientations of the principal stresses proposed by Park et al. [15], the focal mechanism by Kim et al. [7] (Figure 5(b)) is thus consistent with a maximum principal stress oriented at azimuth N64°E (064°) whereas that by Grigoli et al. [6] (Figure 5(c)) is consistent with S76°E (114°). This difference in predicted orientation is substantial, indicating that the predicted stress field orientation is sensitive to modest changes to the focal mechanism of the earthquake. In an attempt to find a solution that is constrained with greater confidence, we consider other options for the relative magnitudes of the principal stresses.

We first investigate the alternative stress field for the Pohang area, proposed by Park et al. [47] using kinematic indicators on Quaternary faults, with $\sigma_V < \sigma_h < \sigma_H$. However, we have misgivings regarding the inclined principal axes of this stress tensor, there being no geological reason why these axes should not be vertical and horizontal in this study region. We suspect that the analysis method used (after [63]) may have produced this inference as an artefact of assumptions made: for example, not all the faults analyzed were dated and some may not reflect the present stress field; or, the stress tensor orientation and/or ratio of principal stresses may vary from fault to fault. Furthermore, Park et al. [47] did not determine absolute principal stresses, only their ratios. We thus consider a modified stress field based on Park et al. [47], with a vertical minimum principal stress and a horizontal maximum principal stress oriented at azimuth 250°. For the representative depth of 4278 m, we retained the lithostatic vertical stress of 110 MPa with a 42 MPa hydrostatic fluid pressure (from [15]). We first chose the principal horizontal stresses to be 200 and 170 MPa to give the "stress ratio" determined by Park et al. [47]. However, this choice of stress field cannot account for the sense of slip in the Pohang earthquake; it predicts rake angles indicative of a lower proportion of right-lateral slip to reverse slip than is observed (Figure 5).

We next consider a revised stress field for the Namsong Fault that can account for the sense of slip, reported by Grigoli et al. [6] for the 15 November 2017 earthquake (Figure 5(c)). Starting from the preceding analysis, for the same 4278 m representative depth, we retain $\sigma_V = 110$ MPa, $\sigma_H = 200$ MPa, and a fluid pressure of 42 MPa, but revise σ_h down to 120 MPa and allow the azimuths of σ_H and σ_h to vary. This focal mechanism is thus consistent with an azimuth of 111° (or S69°E) for σ_H, whereas that in Figure 5(b) would be consistent with 090° (or due east). We also investigate another variant, with $\sigma_V = \sigma_h$. Figure 5(c) would now be consistent with an azimuth of 112° (or S68°E) for σ_H, whereas Figure 5(b) would be consistent with 092° (or S88°E). Taking all these possibilities into account, and acknowledging the uncertainties involved, and that a substantial range of possible stress fields can account for the observed focal mechanism, we will adopt for our analysis of the geomechanics the solution for 4278 m depth with $\sigma_V = 110$ MPa at 111° (or S69°E), $\sigma_H = 200$ MPa, and $\sigma_h = 120$ MPa. We shall also consider, for comparison, the solution for 4200 m depth with $\sigma_V = 106$ MPa at 083° (or N83°E), $\sigma_H = 243$ MPa, and $\sigma_h = 120$ MPa, from [5]. This second alternative model stress field was based on a review of the literature similar to that summarized above, supplemented by new data: dipole sonic logging of well PX-2 in August 2018 revealed anisotropy features at depths between 3.4 and 4.3 km, interpreted [5] to indicate σ_H oriented 077° ± 23° (i.e., between 054° and 100° or between N54°E and S80°E). Both these alternative model stress fields are consistent with the roughly east-west orientation expected for the maximum principal stress beneath Korea (e.g., [55]).

To estimate the orientation of the fractures that undergo "hydroshearing" as a result of the fluid injection, we assume that fractures within the Pohang granite have all possible orientations (cf. Figure 6) and those with preferential orientation relative to the stress field become activated. The preferred geometry for shear reactivation is for fractures with normal vector perpendicular to the intermediate principal stress and at an angle of $45° + \phi/2$ to the maximum principal stress, where ϕ is the angle of friction of the fracture (e.g., [50]). Thus, if the intermediate principal stress is vertical, the reactivated fractures are vertical, but if (as the above analysis suggests) the minimum principal stress is vertical, the reactivated fractures are inclined. Taking the coefficient of friction, c (where $c = \tan(\phi)$), for fractures in granite as ~0.6 (e.g., [64]; granite cuttings from the Pohang wells have c in the range 0.54 to 0.68, with a mean value of 0.63 according to [5]); the preferred orientation for fractures to be sheared has a dip of 30°. If the maximum principal stress azimuth is 111° (see above), these fractures will dip towards either 111° or 291°, whereas if it is 083° (see also above), they will dip towards either 083° or 263°.

We analyze the tendency for coseismic slip in the 15 November 2017 earthquake using the standard Coulomb approach. The Coulomb failure parameter Φ:

$$\Phi = \tau - c(\sigma_N - P_f) - S_C, \quad (1)$$

will thus be evaluated where σ_N, τ, and c are the resolved normal stress, shear stress, and coefficient of friction on the fault plane (or coefficient of internal friction within the rock mass), and P_f and S_C are the fluid pressure and cohesion of the fault zone or rock mass. $\Phi = 0$ marks this condition, with $\Phi < 0$ indicating stability at the point analyzed under the current state of stress. In general, the Coulomb condition for shear failure can also be visualized graphically using the standard Mohr circle construction, which can be plotted on a graph of τ against effective normal stress σ_N', defined as $\sigma_N - P_f$ (Figure 7). Nonetheless, it should be noted that in rocks that are impermeable and fluid pressure only acts in the direction perpendicular to an existing fault, a conventional Mohr circle has no meaning and only points in Mohr circle space that correspond to the orientation of preexisting

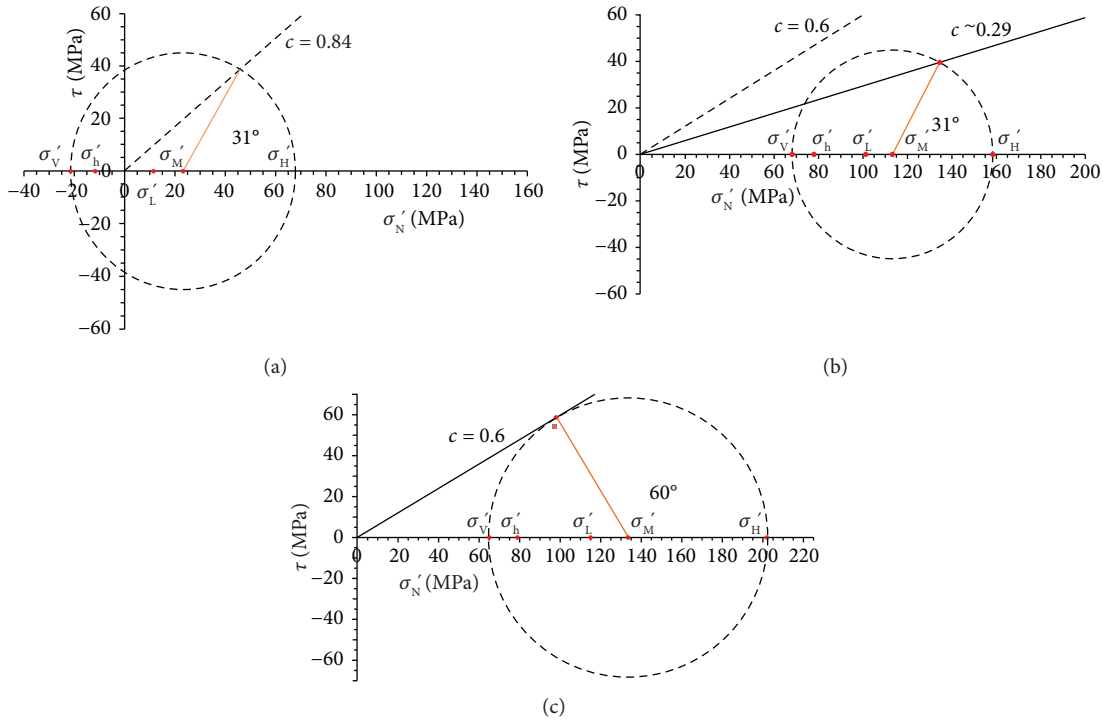

FIGURE 7: Mohr circle representations of the state of stress estimated on the Namsong Fault. The quantities σ_h', σ_H', σ_V', σ_L', and σ_M' denote the effective stresses σ_h-P_f, σ_H-P_f, σ_V-P_f, σ_L-P_f, and σ_M-P_f, where P_f is the fluid pressure at the point for which the analysis is undertaken, $\sigma_L \equiv (\sigma_h + \sigma_H + \sigma_V)/3$, and $\sigma_M \equiv (\sigma_H + \sigma_V)/2$. Inclined line connecting σ_M' to the Mohr circle indicates the orientation—in Mohr circle space—of the pole of the fault. Angles between the maximum principal stress and the normal to the fault plane are labelled (cf. [100, 101]). Failure envelopes are drawn for different values of the coefficient of friction of the Namsong Fault, c. (a) Stress state represented by a lithostatic σ_V of 110 MPa, with $\sigma_h = 120$ MPa and $\sigma_H = 200$ MPa, the latter oriented at an azimuth of 111° to provide consistency with the focal mechanism in Figure 5(c). P_f is set to 132 MPa, the peak value during the initial stimulation of well PX-2 in February 2016 [15]. This diagram indicates that unless $c > 0.84$ the resulting conditions would have caused this fault to slip. Since such a high coefficient of friction is unlikely, it is concluded that this high fluid pressure was not transmitted to the Namsong Fault. (b) For the same depth and stress state as (a) except P_f is set to the hydrostatic value of 42 MPa, to represent the conditions after the injection and flowback experiments in August-September 2017 and before the November 2017 earthquake. Under these conditions c ~0.29 would place the Namsong Fault at the threshold of stability. Also shown for comparison (dashed) is a failure envelope for $c = 0.6$, a representative value for a fault in granite that is unaffected by alteration to authigenic minerals (e.g., [64]). (c) Preferred stress state from [5] for 4200 m depth, represented by a lithostatic σ_V of 106 MPa, with $\sigma_h = 120$ MPa and $\sigma_H = 243$ MPa, the latter oriented at an azimuth of 083°. Under these conditions, $c = 0.6$ would place the Namsong Fault at the threshold of stability for slip in the oblique sense indicated in the focal mechanism in Figure 5(d). A similar plot to this is provided in [5] (their Figure O-11), in which principal stresses of the same magnitudes are oriented slightly differently, with σ_H at an azimuth of 077° rather than 083°. With this adjustment, the focal mechanism in Figure 5(d) is consistent with σ_N' ~97 MPa and τ ~54 MPa; this stress state plots near the threshold for slip for $c = 0.6$ (square symbol in the figure), as was noted in [5].

faults should be considered (e.g., [21, 62]); to emphasize this, the Mohr circles in Figure 7 are drawn dashed. A fault within unaltered granite is expected to have c ~0.6 (e.g., [64]; as already noted, granite cuttings from the Pohang wells have c in the range 0.54 to 0.68, with a mean value of 0.63 according to [5]). Moreover, the Pohang granite has a significant tensile strength (~9 MPa [15]), indicating S_C ~18 MPa; the failure envelope for formation of a new fault will therefore plot (for a given σ_N') at τ ~18 MPa higher than that for a preexisting cohesionless fault.

Figure 7(a) provides an indication of the state of stress at the time of maximum fluid pressure during injection into well PX-2, for the model stress field already discussed, for slip sense indicated by the Grigoli et al. focal mechanism [6]. The fluid pressure at this time was so high that, if the pressure reached the Namsong Fault, this fault would be readily reactivated, even if its coefficient of friction were very high (~0.84). This diagram thus provides clear evidence that this high injection pressure did not directly reach this fault. Nonetheless, with an orientation oblique by ~60° to the maximum principal stress thus indicated, standard frictional considerations (e.g., [65]) indicate (for this stress model and slip sense, in the absence of high fluid pressure) that the Namsong Fault is not at all close to being optimally oriented relative to the local stress field. Moreover, as Figure 7(b) indicates, for a coefficient of friction c as high as 0.6 (and, again, for the slip sense indicated by the Grigoli et al. focal mechanism [6]), the failure envelope passes well outside the Mohr circle for the estimated stress field, predicting stability rather than coseismic slip. Rather than appealing to higher differential stress or above hydrostatic P_f to account for the observed seismicity, it is thus suggested that the Namsong Fault may

have a much lower coefficient of friction; for example, c as low as ~0.2 has been determined for faults in granitic rocks with clay minerals present in fault gouge (e.g., [64]), having plausibly been formed by hydrolysis of plagioclase (see below). A coefficient of friction as low as 0.2 would not be stable under the inferred conditions, but a slightly higher value, ≥0.29, would be consistent with frictional stability.

For comparison, Figure 7(c) illustrates an alternative solution, consistent with the analysis in [5], including their preferred stress state at 4200 m depth (represented by the aforementioned lithostatic $\sigma_V = 106$ MPa, with $\sigma_h = 120$ MPa and $\sigma_H = 243$ MPa) and the slip sense indicated by their focal mechanism in Figure 5(d). Under these conditions, σ_H oriented at an azimuth of 083° would place the Namsong Fault at the threshold of stability for $c = 0.6$. However, this set of parameter values was evidently chosen in [5], from a wide range of possibilities, to be consistent with this stability threshold, rather than it being an independent deduction made directly from evidence. The difference between Figure 7(b) and Figure 7(c) indicates the range of possible conditions that can place the Namsong Fault at the threshold of stability.

3. Water Sampling and Analysis

The August 2017 injection into well PX-1 utilized local surface water, 1756 m^3 being injected. After the injection ended, on 14 August, the experimental protocol required flowback of the injected water. The resulting produced water, 1773 m^3 in total, was repeatedly sampled as progressive compositional changes were anticipated, reflecting varying durations of chemical interaction with the Pohang granite. Given the aforementioned dimensions, the volume of the PX-1 wellbore was 74 m^3 (cased) and 11 m^3 (open-hole), a total of 85 m^3. This means that the last 74 m^3 of water injected, and therefore, the first 74 m^3 produced, remained within the casing and thus had no opportunity to react with the granite.

3.1. Water Sample Collection. Water for this injection experiment was taken from an irrigation pond ~300 m west of the geothermal project site. Water sampled from this pond was analyzed in the field using an Ultrameter II 6PFC hand-held instrument (Myron L Company, Carlsbad, California), which determined water temperature, pH, electrical conductivity (EC), total dissolved solids (TDS), and oxidation-reduction potential (ORP). Five samples were collected for preliminary analysis at site and for subsequent laboratory analysis, three from different parts of the pond and two others from points before and after the filter on the pipe leading to the site. Considerable variability in water composition was thereby demonstrated. Water samples previously collected, before, during, and after previous stimulation experiments, in each of the Pohang wells, were also analyzed using the Ultrameter and retained for laboratory analysis.

Flowback from well PX-1 was initiated at 09:34 (local time) on 14 August 2017; water samples were again collected, the analysis in the field again utilizing the Ultrameter. During the early stages of flowback, the produced water was discharged via a pipe into a mud tank ~10 m from the wellhead. This tank was periodically emptied, and its contents were transported away in tanker lorries for treatment and disposal. Sample collection at this stage involved one of the rig crew (wearing appropriate waterproof and heat-resistant protective clothing) climbing down into the mud tank to access its inlet pipe. Later, after the flow rate decreased, the pipe leading from the wellhead to the mud tank was disconnected and samples were collected directly from the PX-1 wellhead or, during operations to cut the well casing, from a valve in the housing pipe for the casing cutter. The water in the small (1.2 ml) analysis cell of the Ultrameter cooled rapidly, so its initial temperature was underestimated. For many samples, temperature was therefore also read from a thermometer attached to a pole, which one of the rig crew held in the flow. Immediately after collection, samples were taken to a site building where pH and EC were remeasured using a Thermo Scientific Orion Star A329 portable meter (Thermo Fisher Scientific Inc., Waltham, Massachusetts). These replicate measurements were particularly significant on the first day of flowback, because at this stage, the Ultrameter was not correctly calibrated and so yielded incorrect pH and ORP values; it was calibrated using standard buffer solutions in time for the sampling at 10:00 on 15 August.

Rates of injection into well PX-1 were logged at intervals of one minute between the start of injection at 07:00 on 7 August and the end of injection at 09:33 on 14 August. The volume of water injected between these times was thus determined by summation, giving the aforementioned 1756 m^3. Rates of flowback were determined by repeated measurement of changes to the water level in the mud tank, making allowance for the intermittent emptying of this tank as water was removed for treatment and disposal. The resulting measurements were fitted by a polynomial production-decline curve, which has been used here to determine the volume produced at the time of collection of each of the water samples. Flowback began at a rate of ~6.6 l/s but by midnight on August 20, when 1028 m^3 had been produced, had decreased to ~0.5 l/s. The total volume produced, both by "natural" flowback and subsequent pumping, 1773 m^3, thus exceeded the volume injected.

Activity at the site, related to the DESTRESS Horizon 2020 project, officially ended at 19:00 on 16 August. From then on, it was difficult to access the wellhead of well PX-1 for collecting water samples, as the rig crew immediately began to work on other tasks (including installing a casing cutter, cutting the 7" casing at ~800 m depth to install a pump, and extracting the cut casing, leaving surrounding casing with external and internal diameters 9 5/8" and 8 5/8"); for safety reasons, each access required the approval of the site manager and the shift foreman of the rig crew. Water samples collected during this process show short-timescale variations in composition, presumably as a result of mixing of the water being produced with water that had resided within the annulus between the 7" casing, which was cut, and the surrounding cemented casing. Furthermore, removal of the 7" casing increased the volume of the wellbore by ~5 m^3, affecting calculation of the volume

of produced water. After flowback ceased, pumping tests took place within well PX-1; produced water was again sampled during these tests, Ultrameter measurements being made later (in the laboratory), rather than at the site. The supplementary file lists the set of water samples collected and the field measurements made.

3.2. Laboratory Analysis of Water Samples. Anion and cation concentrations were determined simultaneously by ion chromatography using Dionex (Thermo Fisher Scientific Inc., Waltham, Massachusetts) equipment at the School of Engineering of the University of Glasgow. For anions, a 10 μl sample was passed through a Dionex IonPac AG14A guard column and an AS14A-5u analytical column before analysis on an ICS-900 ion chromatography system, with the aid of displacement chemical regeneration suppression (ACRS 500). A mix of 8 mM sodium carbonate/1 mM bicarbonate eluent and 72 mN H_2SO_4 regenerant was pumped through the system at 0.5 ml/min. For cations, a 10 μl sample was passed through a Dionex IonPac CG12A guard column and CS12A analytical column, set to 30°C, before analysis on an ICS-1100 ion chromatography system. Alkalinity was determined as $CaCO_3$ with a Hach Model 16900 digital titrator (Hach Company, Loveland, Colorado), using 0.16 and 1.6 M nitric acid and bromocresol green—methyl red pH indicator. Recorded values were factored by 1.22 to calculate HCO_3^- concentrations. Full details of the analysis methodology are reported elsewhere [66]. Results of this analysis are listed in the supplementary file, along with calculations of the volume of water produced by the times when samples were collected.

3.3. Hydrochemical Description and Interpretation. The pond water used for the August 2017 injection (represented by samples SK01, 02, 03, 20, and 21; see the supplementary file) was relatively fresh (EC 1000-1300 μS/cm), of circumneutral pH, and dominated by Ca-(Na)-SO_4-(Cl) hydrochemistry. The produced water also had a circumneutral pH, but by 1 September, its EC had risen to ~3600 μS/cm, with a composition dominated by sodium and chloride and strongly depleted in magnesium. During the early phases of flowback, the temperature reached a maximum of 65°C (on 17 August; sample SK41; after 823 m^3 of water had been produced), subsequently declining as the flow rate decreased, providing more time for heat loss to the surroundings of the borehole during the ascent of the water. Figure 8 summarizes the variations in character of this produced water in comparison with that injected.

We do not know the exact nature of the "pristine" groundwater, as none of the samples analyzed was collected before injection experiments at the site began. Furthermore, as already noted, during the drilling, fluid was lost into the Namsong Fault, potentially affecting the composition of the groundwater there. We thus investigated the composition of water sampled in 2009 from the Pohang thermal spa resort, ~2 km south of the EGS project site (Figure 2(a)), which utilizes water produced from the Pohang granite via a deep borehole [67]. The properties of this water include temperature 44.0°C, pH 8.4, redox potential 87 mV, electrical conductivity 1977 μS/cm, and concentrations (in mg/l) of K^+ 3.57, Na^+ 536, Ca^{2+} 3.6, Mg^{2+} 1.65, SiO_2 20.1, Li+ 0.23, Sr^{2+} 0.222, HCO_3^- 991.6, F^- 4.58, Cl^- 122, SO_4^{2-} 17.5, and Br^- <0.2 [67]. This water classifies [67] as of Na-HCO_3 hydrochemistry and thus differs significantly from all our samples. Samples of water collected from well PX-2 are different yet again; those collected on 16 March (SK16; before the April 2017 stimulation of well PX-2) and on 27 and 28 August (SK52 and 53; after the August 2017 stimulation of well PX-1 and before the September 2017 stimulation of well PX-2) were much more saline than the waters from well PX-1, being Na-Ca-Cl waters with ~5000 mg/l chloride. The position of the Namsong Fault, with its impermeable core, between wells PX-1 and PX-2 (Figures 2(b) and 3), provides a natural explanation for the significant differences in hydrochemistry of the two sets of water samples; they have been drawn from reservoirs that are hydraulically isolated from each other. The existence of this impermeable "barrier" means that the development plan for this geothermal project, requiring the creation of a hydraulic connection between these two deep wells, was always problematic.

Nonetheless, six samples of water from well PX-1 were collected before the August 2017 stimulation: two (SK19 and 09) in March-April 2017, before and after the April 2017 stimulation of well PX-2, and four (SK10-13) in early August 2017, during well-testing and bleed-off before the August 2017 injection began. These samples are similar to the limiting composition of the samples produced during the flowback following this injection experiment (Figure 8) and thus provide the best estimate of the composition of the groundwater in hydraulic connection with well PX-1 before the August 2017 injection experiment.

Like many granitic intrusions, the Pohang granite consists of quartz, potassic feldspar, plagioclase, and biotite [36]. Potential hydrolysis reactions thus include the dissolution of quartz (e.g., [68])

$$SiO_2\,(s) + 2H_2O\,(l) \leftrightarrow Si(OH)_4\,(aq) \tag{2}$$

and plagioclase (e.g., [69])

$$\begin{aligned} &NaCaAl_3Si_5O_{16}\,(s) \\ &\quad + 4H_2O\,(l) + 12H^+\,(aq) \leftrightarrow Na^+\,(aq) + Ca^{2+}\,(aq) \\ &\quad + 3Al^{3+}\,(aq) + 5Si(OH)_4\,(aq) \end{aligned} \tag{3}$$

or the hydrolysis of plagioclase to produce the hydrous clay mineral smectite (montmorillonite) (e.g., [64])

$$\begin{aligned} &2NaCaAl_3Si_5O_{16}\,(s) \\ &\quad + (3n-4)H_2O\,(l) \\ &\quad + 6H^+\,(aq) + 2Si(OH)_4\,(aq) \rightarrow 3Al_2Si_4O_{10}(OH)_2.n(H_2O)\,(s) \\ &\quad + 2Ca^{2+}\,(aq) + 2Na^+\,(aq). \end{aligned} \tag{4}$$

Other reactions can include the precipitation of Mg^{2+} and

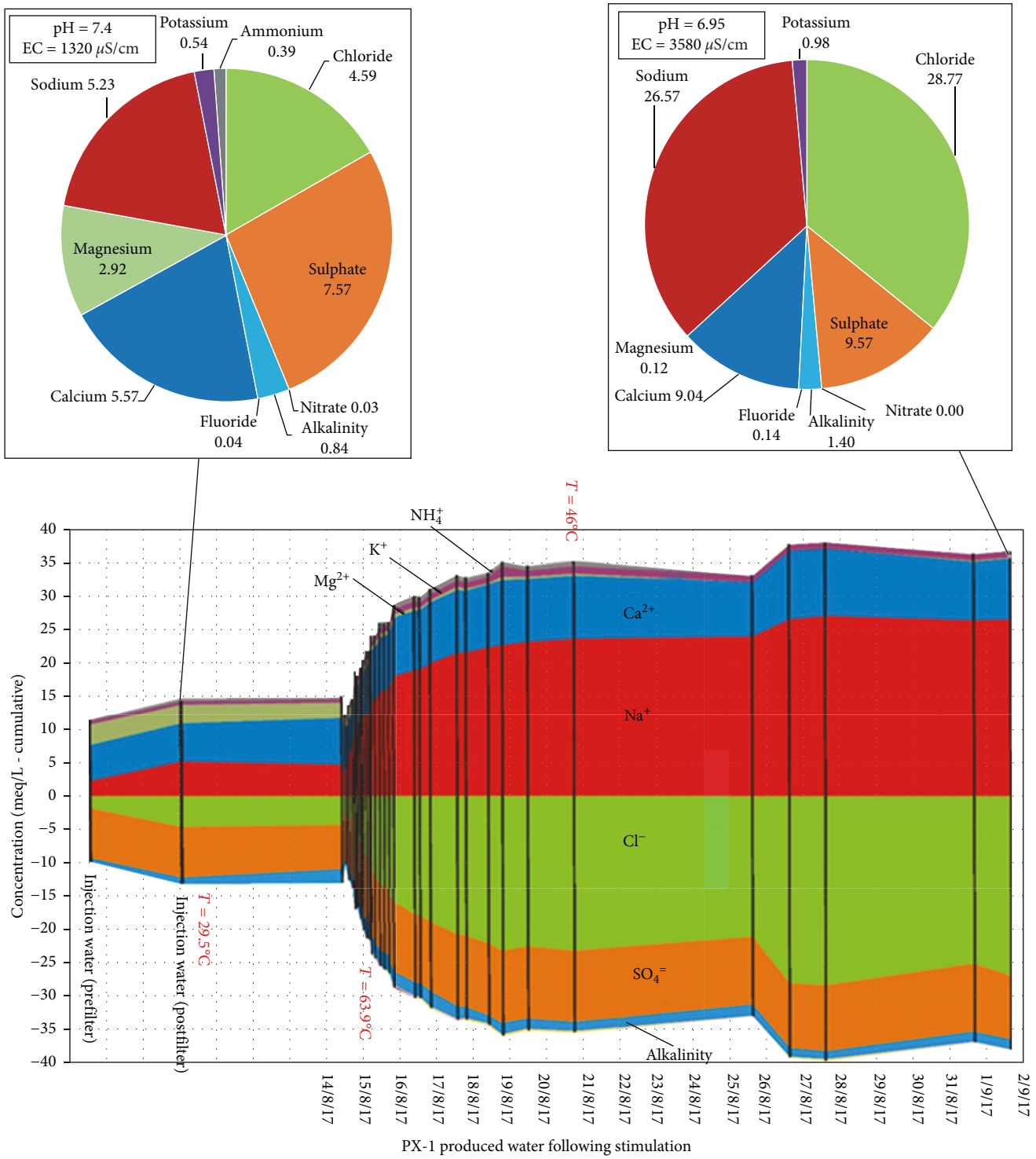

Figure 8: Summary of variations over time in the composition and other properties of the water injected into, and subsequently produced from, well PX-1 in August 2017, using data from the supplementary file.

associated uptake into solution of Ca^{2+} during alteration of primary igneous minerals to clay minerals and chlorite (e.g., [70]). Equilibrium concentrations of dissolved quartz have been calculated using PhreeqcI version 3.3.5 software (U.S. Geological Survey, Reston, Virginia) with phreeqc.dat internal database [71]. It is thus 6.3 mg of SiO_2 per litre under near-surface conditions (pressure 0.3 MPa; temperature 25°C; density of water 997 kg m^{-3}) and 186 mg of SiO_2 per litre at 4300 m depth (pressure 416 atm or 42.2 MPa; temperature 160°C; density of water 930 kg m^{-3}).

Multiple characteristics of the limiting composition of the produced water and of the waters sampled from well

PX-1 before its August 2017 stimulation (e.g., its Na^+/Cl^- and Br^-/Cl^- ionic ratios) resemble seawater (Figures 9 and 10). As recently as the Middle Miocene [72], this locality was submerged beneath the sea, during deposition of mudstone (the Yeonil Group; Table 1), which crops out locally; we infer that pervasive circulation of seawater through the granite, dating from this time, established this composition, which we thus deduce indicates the "natural" groundwater within the granite. Conversely, other properties differ from those of seawater, providing clear evidence of water-rock interaction, for example, the low Mg^{2+}/Ca^{2+} and high SO_4^{2-}/Cl^- ratios, potentially explicable as consequences of increased Ca^{2+} from dissolution of plagioclase or from ion exchange associated with precipitation of Mg^{2+} during hydrolysis of other igneous minerals to clay minerals and chlorite, and increased SO_4^{2-} from oxidation of pyrite, FeS_2. Such complexity, indicating interactions between the rock and water that originated as meteoric water or palaeoseawater, has been recognized previously in hot spring waters from SE Korea (e.g., [67, 73]).

The variations in composition (e.g., for SO_4^{2-}/Cl^- and Na^+/Cl^-; Figure 10) can be approximated as indicating production of an initial ~100 m^3 of surface water, followed by ~400 m^3 of water that provides evidence of water-rock reaction, reflected in the elevated Na^+/Cl^- ratios, followed by production of a large volume of water that is similar to, if not indistinguishable from, the preexisting groundwater. This Na^+/Cl^- "spike" reflects an excess of Na^+ ions in the produced water, which we attribute to hydrolysis by the injected water of plagioclase within the granite (cf. [69]). Approximating the pattern crudely as indicating the proportion of surface water to groundwater decreasing linearly from 100% to 0% as the produced volume increases from 100 to 500 m^3, the volume of surface water recovered by flowback can be roughly estimated as ~300 m^3; given the 1756 m^3 of surface water injected, this implies that ~1400 m^3 of the injected surface water remained in the subsurface at the end of the flowback.

4. Hydrochemical/Geomechanical Model

The hydrochemical dataset presented in Figures 8–10 indicates that well PX-1 is hydraulically connected to the groundwater within the granite. Moreover, although the volume of water produced from well PX-1 roughly equalled that injected in August 2017, because much of the produced water was "natural" groundwater, it follows that much of the injected surface water (~1400 m^3 or ~80%) remained within the granite. Figure 11 illustrates a conceptual model that might thus account for the 15 November earthquake. It assumes that the August 2017 injection into well PX-1 indeed enhanced fracture permeability downward, releasing surface water into the Namsong Fault. Subsequent flowback drew water from this fault: initially, injected surface water; subsequently, a mixture of surface water and groundwater; and, ultimately, groundwater, thus leaving a "pocket" of surface water "trapped" within the fault.

A major fault such as the Namsong Fault can be inferred to have a complex structure, as detailed in Figure 4. Much work has been carried out on interactions between fluids within faults and earthquake processes (e.g., [74, 75]). A fault can thus be regarded as consisting of "patches" in frictional contact, "asperities," which provide frictional strength, separated by volumes occupied by fluid (as in Figure 12). This fluid is usually at its equilibrium concentration; pressure solution resulting from the normal stress across a fault thus dissolves the tips of asperities, which are in contact, causing reprecipitation around their edges, widening the area in contact and strengthening the fault [74]. However, if the fluid is not in chemical equilibrium, as in Figures 11(d) and 11(e), dissolution at asperities will not be accompanied by reprecipitation elsewhere. Dissolution of a thin layer at any asperity will create space to enable the fault wall rocks to decompress towards the fault, reducing the compressive normal stress and "unclamping" the fault.

Although our data (Figure 10) indicate mineral hydrolysis or dissolution (probably of plagioclase), we have no direct evidence for hydrolysis of quartz, as silica has not been measured in our water samples. However, this can be inferred by comparison of the rate constants for hydrolysis of plagioclase and quartz (cf. [68, 69]). At the ~160°C bottom-hole temperature at Pohang, the equilibrium concentration of dissolved silica is several hundred mg/l; timescales for reequilibration of silica as a function of temperature, in fractures of a given width, are shown in Figure 13. Chemical reequilibration of water within a fault thus provides a mechanism for postinjection anthropogenic seismicity, with a time delay governed by the dissolution rate. Provided this process is governed by the kinetics of hydrolysis of quartz, Figure 13 indicates that at 160°C a three-month duration of hydrochemical and stress reequilibration, and thus a three-month delay of postinjection seismicity, is feasible for a fault of a typical width $W = 0.6$ mm.

The magnitude M_W and seismic moment M_O of the largest earthquake that might thus be caused, after a volume V of surface water becomes "trapped" within a fault (cf. Figure 11(d)), can also be estimated. We adopt a conceptual model of a fault as illustrated in Figure 12. The model fault is assumed permeable, with a typical width W, and filled by fluid, the bounding rocks being impermeable. If the fault thus occupied has a square cross-section of side length L, then $V = W \times L^2$. If this area of fault slips, then from standard theory (e.g., [76]) $M_O = \mu \times u \times L^2$, and the stress drop $\Delta\sigma = \mu \times u/L$, μ being the shear modulus of the adjoining rocks and u the spatial average coseismic slip. Combining these equations gives

$$M_O = \Delta\sigma \times \left(\frac{V}{W}\right)^{3/2}. \quad (5)$$

M_W can be calculated from M_O using the standard equation

$$\log_{10}(M_O/\mathrm{N\,m}) = 9.05 + 1.5 \times M_W \quad (6)$$

[77]. Taking $V = 1400$ m^3 for the August 2017 injection, $W = 0.6$ mm (Figure 13), and $\Delta\sigma = 10$ MPa (an upper

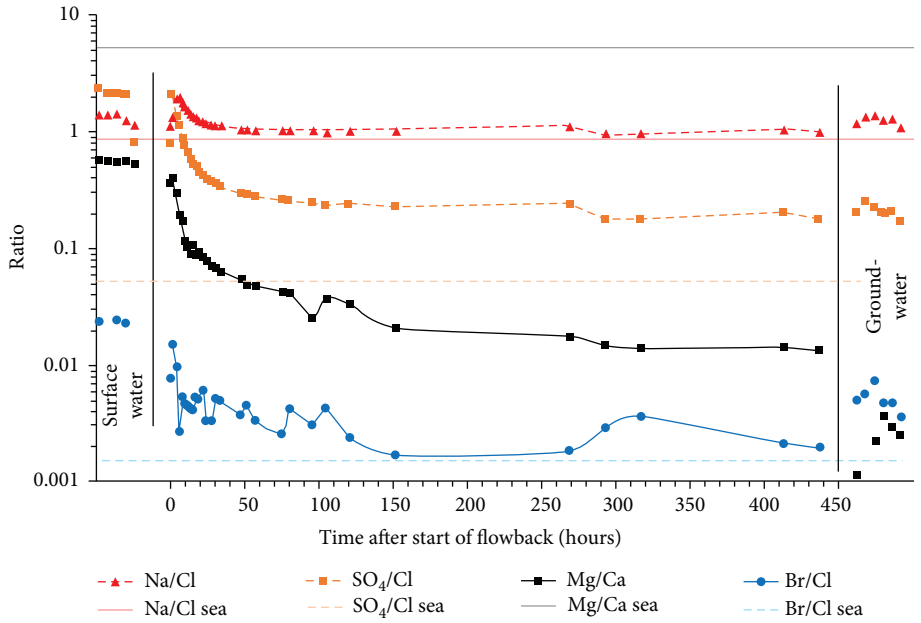

Figure 9: Variations in molar ionic ratios for the water produced from well PX-1 in August-September 2017, compared with equivalent ratios for seawater and for samples of the surface water used for injection (samples SK01-03 and SK20-21) and of groundwater previously recovered from well PX-1 (samples SK09-13 and SK19). Data for all samples are from the supplementary file. Calculations here and for Figure 10 use molar masses: Ca^{2+}, 40.08 g; Mg^{2+}, 24.305 g; Na^{+}, 22.99 g; Br^{-}, 79.9 g; Cl^{-}, 35.453 g; and SO_4^{2-}, 96.06 g. Comparisons with seawater are based on a notional representative composition of seawater, defined as the mean of the Lenntech [102] and Stanford University [103] standards.

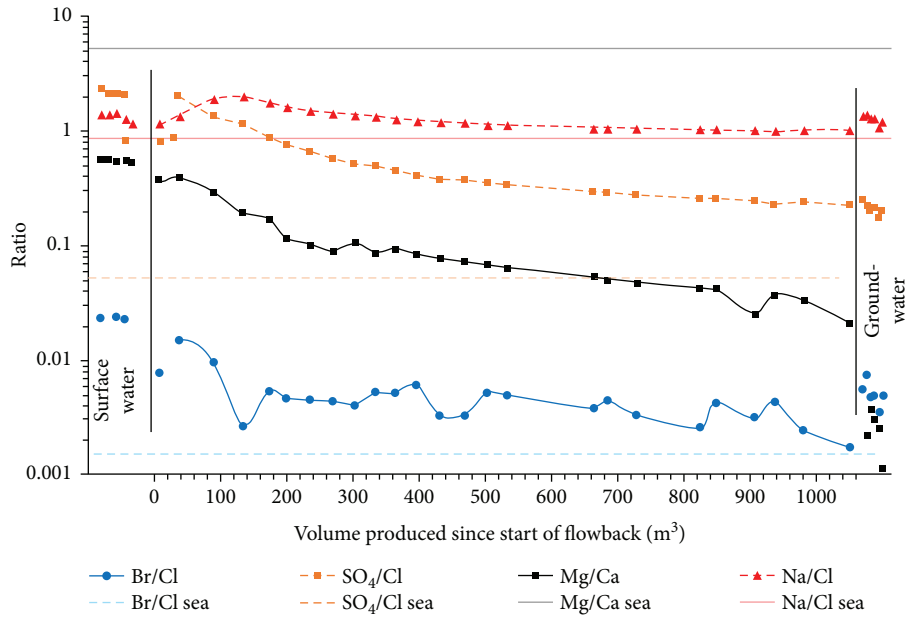

Figure 10: The same hydrochemical data as in Figure 9, for water produced from well PX-1 during August-September 2017, compared with five analyses of the surface water used as the source and six analyses indicative of the composition of preexisting groundwater in this well, but plotted as a function of the volume of produced water rather than as a function of time. Patterns, as flowback proceeds, include the tenfold decrease in the SO_4^{2-}/Cl^{-} ratio, in a manner explicable by mixing of a progressively greater proportion of groundwater with a progressively smaller proportion of surface water. Conversely, the Na^{+}/Cl^{-} ratio is similar in the surface water and groundwater, thus insensitive to mixing, but "spikes" by a factor of ~2 during the initial ~500 m^3 or ~30 hours of flowback, this variation being explicable as a result of reaction between the injected water and the granite. Note that the first 74 m^3 of produced water remained within the casing of well PX-1 after injection and so did not interact with the Pohang granite.

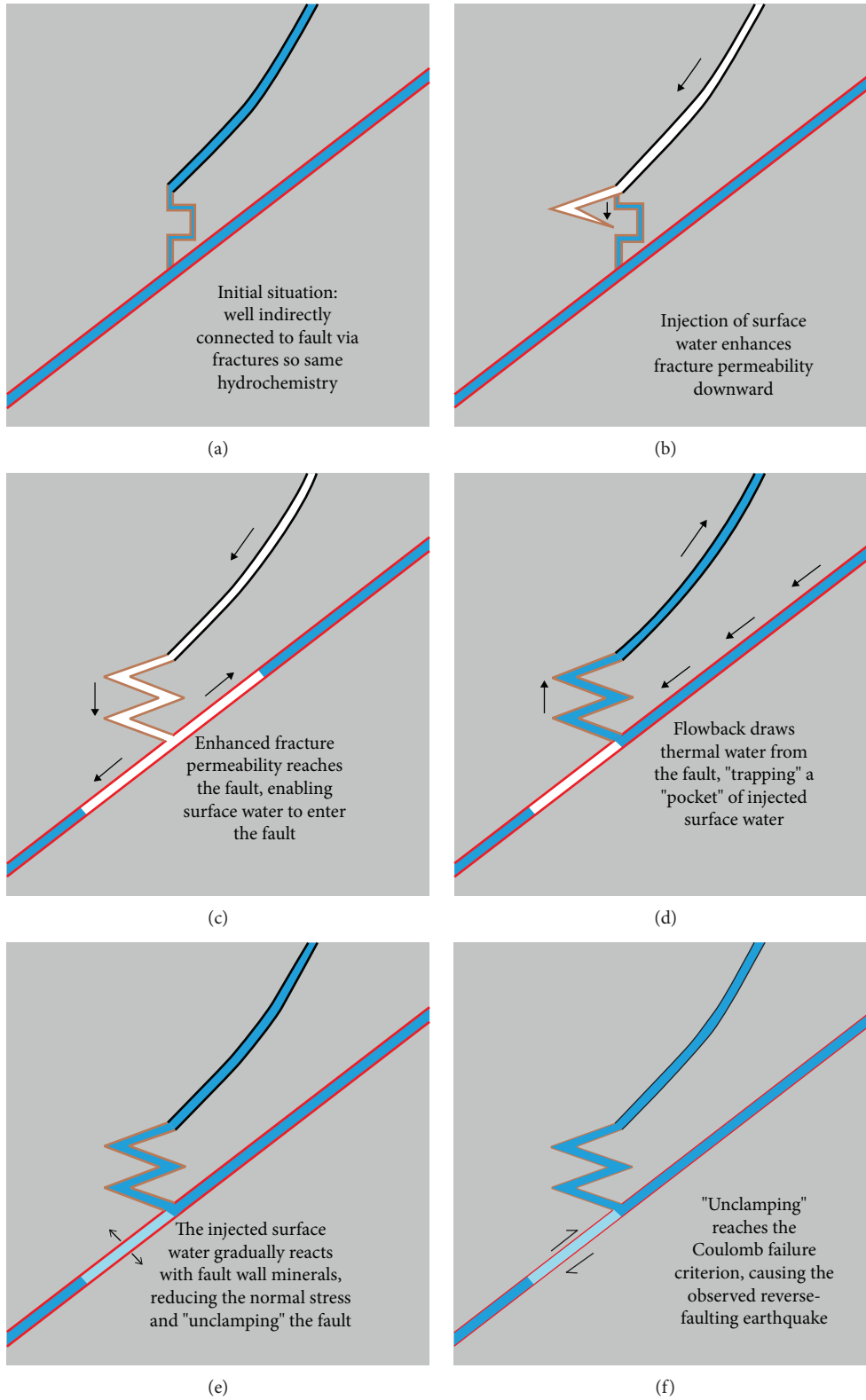

Figure 11: Conceptual model linking injection into well PX-1 to the 15 November 2017 earthquake. Panels depict NW-SE cross-sections across the Namsong Fault (cf. Figure 2(b)), not to scale. The "zig-zag" pattern of fracturing reflects the analysis indicating a preferred orientation, given the local stress field, at 30° dip towards S69°E or N69°W, or towards N83°E or S83°W, depending on the choice of model stress field. Using standard theory, the largest earthquake in August 2017 (M_W 1.9; [17]) would correspond to shearing of a fracture with dimensions no greater than ~50 m, indicating the probable upper bound to the individual "zig-zag" fracture segments. See text for discussion.

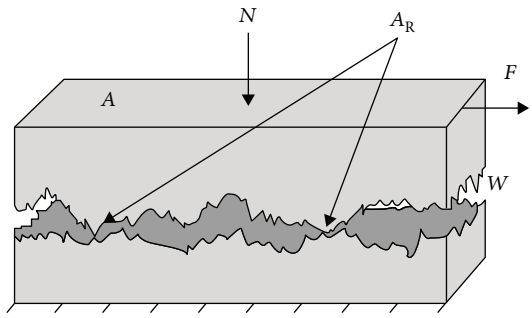

Figure 12: Conceptual model for a fault, modified after [81]. The fault is regarded as a fluid-filled volume of area A and typical width W, its surfaces—with fractal distributions of irregularities—being in contact at asperities of area A_R, with $A_R \ll A$. N and F are the normal and shear forces acting across the fault, associated with the normal and shear stresses σ_N and τ. This model simplifies the features depicted in Figure 4 for calculation purposes.

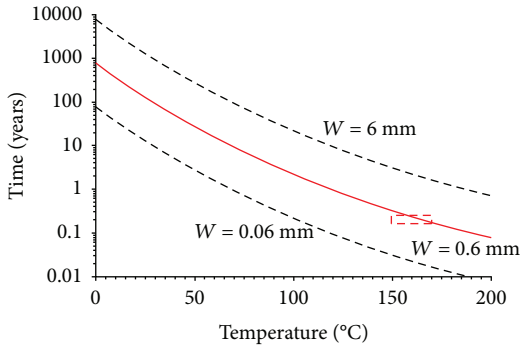

Figure 13: Timescales for equilibration of concentration of dissolved silica (i.e., $Si(OH)_4$) in fractures of width W (where $W = 0.06$, 0.6, and 6 mm), after Rimstidt and Barnes [68]. Calculations assume $Si(OH)_4$ concentrations of zero, initially, increasing to 99.3% of the equilibrium value, thus depicting five times the "time constant" for the dissolution. Box represents a 160 ± 10°C temperature and a 2-3 month timescale, consistent with the bottom-hole temperature and postinjection time-delay observed at Pohang in 2017.

bound; e.g., [78, 79]), one obtains $M_O = 4 \times 10^{16}$ N m and $M_W = 5.0$, in a reasonable agreement with the observed $M_W = 5.5$. Taking $V = 2800\,m^3$, to allow for the possibility that an equal volume of surface water remained underground after the December 2016-January 2017 injection into well PX-1, but keeping the other parameter values the same gives $M_O = 1 \times 10^{17}$ N m and $M_W = 5.3$. Calculation assuming $V = 80\%$ of the overall injected ~12,000 m^3 [5, 17], or ~10,000 m^3, gives $M_O = 7 \times 10^{17}$ N m and $M_W = 5.9$.

For comparison, existing theory [9] predicts

$$M_O = \mu \times V, \tag{7}$$

(with V now denoting the net volume injected) thus giving (in granite with $\mu = 20$ GPa) $M_O = 4 \times 10^{13}$ N m and $M_W = 3.0$ for injected volume $V = 1756\,m^3$ or $M_O = 2 \times 10^{14}$ N m and $M_W = 3.6$ for $V = 12{,}000\,m^3$ (or even lower values of M_O and M_W if one uses net injected volumes at Pohang, taking into account volumes of water subsequently produced). However, the derivation of this theory [9] assumes that the injected water floods pore-space in the rock volume surrounding a fault rather than being localized within the fault; this assumption is inappropriate for injection into granite that has essentially zero porosity and permeability except within faults and fractures.

The rocks bounding the model fault in Figure 12 are assumed to be held in frictional contact at asperities, which are assumed to follow a fractal size distribution; this means that they occupy the area A_R that is proportional to the effective normal stress σ_N' (e.g., [80, 81]), such that

$$A_R = k\sigma_N' A, \tag{8}$$

A being the overall fault area. Dissolution of these fault wall rocks, of density ρ_R, in response to chemical disequilibrium within this fluid, is assumed to be localized at these asperities (as a result of pressure solution; cf. [74]), and to remove a thickness δW of rock from each as the fluid reequilibrates. The mass of rock that dissolves is thus $\rho_R \times A_R \times \delta W$. This can be equated to the mass of material entering solution which will be $C \times A \times W$ if its concentration in the volume $A \times W$ increases from zero to C; one thus obtains

$$\frac{\delta W}{W} = \frac{C}{\rho_R k\sigma_N'}. \tag{9}$$

As the asperities dissolve, the fault wall rocks will decompress towards the fault, moving inward on either side by distance $\delta W/2$, thus reducing the effective normal stress on the fault by $\delta\sigma_N'$ where

$$\delta\sigma_N' = \frac{E\delta W}{2D}, \tag{10}$$

D being the width (perpendicular to the fault) of the adjoining blocks and E their Young's modulus. Thus,

$$\delta\sigma_N' = \frac{ECW}{2D\rho_R k\sigma_N'}. \tag{11}$$

To apply this analysis to Pohang, we take $E = 50$ GPa (nominal value for granite), $k\sigma_N' = \sim 0.03$ (from [81]), from a numerical simulation of a fault with fractal roughness, for $\sigma_N' \sim 135$ MPa after Figure 7, $\rho_R = 2650\,kg\,m^{-3}$ for quartz, $C \sim 200\,mg\,l^{-1}$ for dissolution of quartz under the conditions at Pohang (from the earlier calculation using PhreeqcI), $W = 0.6$ mm (from the present analysis of the time delay for the induced seismicity; Figure 13), and $D \sim 0.5$ m (cf. Figure 6), obtaining ~80 kPa for $\delta\sigma_N'$. If the Namsong Fault was already very close to the Coulomb condition for slip stability, as in Figures 7(b) or 7(c) (depending on the choice of local stress field model and slip sense in the M_W 5.5 earthquake), a small change in σ_N' such as this might cause for slip

instability. Regardless of the choice of stress field model and slip sense, the relatively small magnitude of this change to the state of stress means that this fault must have already been very close to the condition for slip for this mechanism to explain the seismicity. Nonetheless, from equation (11), the predicted value of $\delta\sigma_N{}'$ is proportional to W. Thus, for example, if the chemical disequilibrium within the Namsong Fault was caused by the first stimulation of well PX-2, starting in January 2016, the delay of ~1.8 years indicates W ~5 mm, giving $\delta\sigma_N{}'$ ~0.6 MPa. If caused by the aforementioned loss of circulation into the fault during the drilling of well PX-2 in November 2015 [5], the ~2-year delay indicates similar values for W and $\delta\sigma_N{}'$. Furthermore, if the disequilibrium was caused by the loss of circulation into the fault during the drilling of well PX-1, with its original vertical orientation, in the autumn of 2013 [16], the ~4-year delay indicates W ~10 mm, predicting $\delta\sigma_N{}'$ ~1.2 MPa. These calculations omit any cooling effect of the injected water, on the basis that any such effect will be minor (with duration much less than these timescales), in accordance with earlier discussion.

Nonetheless, this mechanism can only account for small changes in the state of stress on a fault, by ≤~0.1 MPa for the analysis relating to the August 2017 injection into well PX-1, implying that the Namsong Fault must already have been very close to the condition for slip. Given the interrelationships between W, temperature, and time delay (Figure 13), an anthropogenic earthquake with $M_W > 5.0$, with a shorter delay, might be predicted in rocks at 160°C for $V = 1400\ m^3$ for a fault with $W < 0.6$ mm, although it requires the fault to already be even closer to the slip condition. Conversely, a longer delay might result for a fault with larger W, enabling a greater change in the stress state to the slip condition, although from equation (5) the largest earthquake feasible after a longer delay, for a given injected volume, would be smaller; furthermore, injection into a wider fault might in principle cause significant cooling (as noted above), slowing the hydrochemical reactions and prolonging the time delay (cf. Figure 13).

5. Discussion

This analysis indicates that hydrochemical "corrosion" following injection of water into granite, under conditions that make the water silica undersaturated, can affect the state of stress on a fault on subsequent timescales of months, potentially years, bringing the fault closer to the condition for slip. The analysis might be developed to incorporate hydrolysis of other minerals. Nonetheless, this mechanism can only cause seismicity on a fault already close to the condition for slip (i.e., critically stressed). It is widely accepted that intraplate continental crust is indeed critically stressed, meaning that in each region, the faults most favourably oriented to the stress field lie close (within one earthquake stress drop, or ≤10 MPa; e.g., [78, 79]) to the slip condition (e.g., [82–84]). The small magnitude predicted for the hydrochemical changes to the stress state at Pohang indicates that the Namsong Fault was already extremely close to slipping. It is noted in passing that much published discussion of "critically stressed'" crust, meaning crust containing faults that are within one earthquake stress drop of the Coulomb failure condition, assumes that "Byerlee's Law" is applicable to these faults (i.e., they are subject to hydrostatic fluid pressure and have a coefficient of friction of ~0.6 [85]). However, these are really two separate concepts: as already noted, faults lined with clay minerals can have coefficients of friction as low as ~0.2 (e.g., [64]), a point that was indeed noted in the classic paper by Brace and Kohlstedt [85] that defined "Byerlee's Law" in the first place, but might still be "critically stressed" (i.e., be within one earthquake stress drop of the Coulomb failure condition). The present deduction that the Namsong Fault is critically stressed is thus independent of any inference regarding the coefficient of friction of this fault. This case study indeed highlights the importance of establishing whether faults adjoining other EGS sites are critically stressed, before injection takes place.

Like poroelasticity, this hydrochemical "corrosion" mechanism has the potential to account for seismicity after significant time delays following fluid injection. This mechanism has been shown in the preceding calculations to be able to account for changes in the state of stress on the Namsong Fault, by the time of the 15 November 2017 earthquake, that are at least as large, and possibly larger, than the ~80 kPa effect of poroelasticity previously estimated [5]. Although only the hydrochemical consequences of the August 2017 injection experiment have been analyzed in any detail, this mechanism will have a cumulative effect on the state of stress throughout the programme of injection experiments in each of the wells and over time thereafter. From this point of view, this mechanism differs from the poroelastic effect on the state of stress following each injection experiment, which will ultimately dissipate leaving no permanent effect. Although cyclic stimulation was adopted for the August 2017 injection experiment in an attempt to mitigate induced seismicity [17], this technique will have no mitigating effect on seismicity caused by hydrochemical "corrosion." However, in principle (setting aside issues of cost), the latter effect could be mitigated by injecting water that is in chemical equilibrium with the preexisting groundwater at the injection point. This might be achieved by injecting local groundwater or treating surface water before injection to increase the concentrations of dissolved ionic species to mimic the composition of local groundwater. The effect might also be mitigated through geophysical and geomechanical investigations to identify any large, critically stressed faults in the vicinity of any fluid injection site, prior to injection taking place. The March 2019 report to the Republic of Korea government [5] offers other recommendations regarding the governance of future EGS projects.

The preliminary analysis of hydrochemical "corrosion," presented here, can be developed through analysis and modelling of changes to the concentration of additional ionic species. Such work is beyond the scope of the present study and will be presented elsewhere. A related additional task, also beyond the scope of the present study, is to develop the present conceptual model of a fault (Figure 13) to incorporate the complexity of actual fault zones, notably the distinction between impermeable fault core and permeable damage

zone (cf. Figures 3 and 4). Preliminary models of fault zones have envisaged a central fault core with damage zones of an equal width on either side (e.g., [86, 87]). However, where transected by well PX-2, the Namsong Fault is asymmetric, with its damage zone on the footwall side of the fault core (Figure 3). Such asymmetry has been noted on other faults, along with complex lateral variations in the disposition of the damage zone relative to the fault core on a variety of scales (e.g., [88–91]). It is thus feasible for the damage zone of the Namsong Fault to be differently disposed below well PX-1, either symmetrically about the fault core or concentrated in its hanging wall, thus making this part of this fault potentially susceptible to hydrochemical "corrosion" following injection into well PX-1. For example, the theory presented here might be adapted to reflect observations of fault damage zones that indicate multiple subparallel fractures, with a characteristic spatial frequency F that depends on factors such as lithology and fault displacement (e.g., [88]); the theory might thus be refined by associating the parameter D, as currently defined, with 1/F. A further refinement might be to recognize the tensile nature of secondary fractures that are oriented obliquely to faults in granite [92]; the width of these will contribute to the overall value of the parameter W, in addition to the direct contribution of fault-parallel shear zones in any "transitional zone" bounding the impermeable fault core (cf. [88]; Figure 4). Elaborations such as these, beyond the scope of the present study, will be addressed in future research.

6. Conclusions

The 15 November 2017 M_W 5.5 Pohang earthquake occurred months after the most recent injection of surface water into granite as part of development of the Pohang EGS project. Having noted that most of the water produced by flowback, following the injection experiment in August 2017, was originally groundwater, and that much of the injected surface water therefore remained in the subsurface; we have investigated the possibility that hydrochemical "corrosion" of the granite by the injected surface water contributed to the earthquake. To test this possibility, we have derived a theory linking the postinjection time delay of the seismicity to the temperature at depth by considering the kinetics of dissolution of quartz within the granite and linking the volume of surface water that remains in the subsurface to the seismic moment of the resulting earthquake. We thus show that at a temperature of 160°C, the retention in the subsurface of 1400 m^3 of surface water, injected in August 2017, can change the state of stress of a fault that is typically 0.6 mm wide by ~80 kPa and can thus cause an earthquake of seismic moment as large as 4×10^{16} N m, with M_W 5.0. Surface water injected at other times, or drilling fluid that entered the fault when it was transected during drilling, may well have also contributed to "corroding" this fault, explaining why the earthquake was somewhat larger than is predicted by this theory. The new theory predicts a significantly larger upper bound to the seismicity that might result from a given volume of fluid injection compared with existing theory [9], as a result of the different assumptions made: the injected fluid is assumed to only occupy the seismogenic fault rather than flooding the surrounding rock volume. For the small calculated change to the state of stress to have resulted in an earthquake, the Namsong Fault must have already been critically stressed, i.e., very close to the condition for slip. The proposed "hydrochemical corrosion" mechanism is thus shown to be a plausible candidate, in this instance, demonstrating the need to consider this mechanism for future EGS projects in granite. This case study also highlights the importance of establishing whether faults adjoining EGS sites are critically stressed before injection takes place.

Data Availability

The hydrochemical data used to support the findings of this study are included within the supplementary information file.

Conflicts of Interest

The authors declare that there is no conflict of interest regarding the publication of this paper.

Acknowledgments

Anne McGarrity ran the hydrochemical analyses. We thank many DESTRESS coworkers, especially Günter Zimmermann and David Banks, for helpful discussions. We would like to thank Art McGarr for thoughtful and constructive review comments. We dedicate this work to the memory of our colleague, Paul Younger (1 November 1962–21 April 2018), who instigated University of Glasgow involvement in DESTRESS and secured the funding for this work. The authors are funded in part by European Commission Horizon 2020 project EC-691728, DESTRESS (DEmonstration of soft Stimulation TREatmentS of geothermal reservoirS). NMB is also funded by a University of Glasgow Lord Kelvin/Adam Smith Research Fellowship.

Supplementary Materials

Supplementary Materials. The supplementary file lists the results of field analysis and laboratory analysis of water samples from Pohang. *(Supplementary Materials)*

References

[1] S. Wiemer, T. Kraft, and D. Landtwing, "Seismic risk," in *Energy from the Earth: Deep Geothermal as a Resource for the Future? TA Swiss Geothermal Project Final Report*, S. Hirschberg, S. Wiemer, and P. Burgherr, Eds., Paul Scherrer Institute, Villigen, Switzerland, 2014.

[2] J. L. Rubinstein and A. B. Mahani, "Myths and facts on wastewater injection, hydraulic fracturing, enhanced oil recovery, and induced seismicity," *Seismological Research Letters*, vol. 86, no. 4, pp. 1060–1067, 2015.

[3] E. Trutnevyte and O. Ejderyan, "Managing geoenergy-induced seismicity with society," *Journal of Risk Research*, vol. 21, no. 10, pp. 1287–1294, 2017.

[4] C. D. Klose, "Mine water discharge and flooding: a cause of severe earthquakes," *Mine Water and the Environment*, vol. 26, no. 3, pp. 172–180, 2007.

[5] K.-K. Lee, I.-W. Yeo, J.-Y. Lee et al., "Summary report of the Korean Government Commission on relations between the 2017 Pohang earthquake and the EGS project," in *Geological Society of Korea and Korean Government Commission on the Cause of the Pohang Earthquake*, p. 205, Seoul, Republic of Korea, March 2019, http://www.gskorea.or.kr/custom/27/data/Summary_Report_on_Pohang_Earthquake_March_20_2019.pdf.

[6] F. Grigoli, S. Cesca, A. P. Rinaldi et al., "The November 2017Mw5.5 Pohang earthquake: A possible case of induced seismicity in South Korea," *Science*, vol. 360, no. 6392, pp. 1003–1006, 2018.

[7] K.-H. Kim, J. H. Ree, Y. H. Kim, S. Kim, S. Y. Kang, and W. Seo, "Assessing whether the 2017Mw5.4 Pohang earthquake in South Korea was an induced event," *Science*, vol. 360, no. 6392, pp. 1007–1009, 2018.

[8] M. Zastrow, "South Korea's most-destructive quake probably triggered by geothermal plant," *Nature*, 2018, https://www.nature.com/articles/d41586-018-04963-y.

[9] A. McGarr, "Maximum magnitude earthquakes induced by fluid injection," *Journal of Geophysical Research, Solid Earth*, vol. 119, no. 2, pp. 1008–1019, 2014.

[10] M. Zastrow, "South Korea accepts geothermal plant probably caused destructive quake," *Nature*, 2019, https://www.nature.com/articles/d41586-019-00959-4.

[11] Y. Song, S. K. Lee, H. C. Kim et al., "Case study on a low-enthalpy geothermal exploration in Pohang area, Korea," *Geosystem Engineering*, vol. 6, no. 2, pp. 46–53, 2003.

[12] T. J. Lee, Y. Song, and T. Uchida, "Two-dimensional interpretation of far-remote reference magnetotelluric data for geothermal application," *Geophysical Exploration*, vol. 8, pp. 145–155, 2005.

[13] T. J. Lee, Y. Song, D.-W. Park, J. Jeon, and W. S. Yoon, "Three dimensional geological model of Pohang EGS pilot site, Korea," in *Proceedings, World Geothermal Congress 2015*, vol. 19no. 25, p. 6, Melbourne, Australia, April 2015.

[14] T. J. Lee, Y. Song, W. S. Yoon et al., "The first enhanced geothermal system project in Korea," in *Proceedings of the 9th Asian Geothermal Symposium*, vol. 7, p. 9, Kagoshima, Japan, November 2011.

[15] S. Park, L. Xie, K.-I. Kim et al., "First hydraulic stimulation in fractured geothermal reservoir in Pohang PX-2 well," *Procedia Engineering*, vol. 191, pp. 829–837, 2017.

[16] K.-S. Yoon, J.-S. Jeon, H.-K. Hong et al., "Deep drilling experience for Pohang enhanced geothermal project in Korea," in *Proceedings, World Geothermal Congress*, vol. 19, Melbourne, Australia, April 2015.

[17] H. Hofmann, G. Zimmermann, M. Farkas et al., "First field application of cyclic soft stimulation at the Pohang enhanced geothermal system site in Korea," *Geophysical Journal International*, vol. 217, no. 2, pp. 926–949, 2019.

[18] J.-H. Choi, K. Ko, Y. S. Gihm et al., "Surface deformations and rupture processes associated with the 2017 M_W 5.4 Pohang, Korea, earthquake," *Bulletin of the Seismological Society of America*, vol. 109, no. 2, pp. 756–769, 2019.

[19] S. D. Davis and C. Frohlich, "Did (or will) fluid injection cause earthquakes? - criteria for a rational assessment," *Seismological Research Letters*, vol. 64, no. 3-4, pp. 207–224, 1993.

[20] R. Davies, G. Foulger, A. Bindley, and P. Styles, "Induced seismicity and hydraulic fracturing for the recovery of hydrocarbons," *Marine and Petroleum Geology*, vol. 45, pp. 171–185, 2013.

[21] R. Westaway, "Integrating induced seismicity with rock mechanics: a conceptual model for the 2011 Preese Hall fracture development and induced seismicity," *Geological Society, London, Special Publications*, vol. 454, no. 1, pp. 327–359, 2017.

[22] J. K. Costain, "Groundwater recharge as the trigger of naturally occurring intraplate earthquakes," *Geological Society, London, Special Publications*, vol. 432, no. 1, pp. 91–118, 2017.

[23] P. Segall, "Earthquakes triggered by fluid extraction," *Geology*, vol. 17, no. 10, pp. 942–946, 1989.

[24] P. Segall, J.-R. Grasso, and A. Mossop, "Poroelastic stressing and induced seismicity near the Lacq gas field, southwestern France," *Journal of Geophysical Research*, vol. 99, no. B8, pp. 15423–15438, 1994.

[25] K. W. Chang and P. Segall, "Injection-induced seismicity on basement faults including poroelastic stressing," *Journal of Geophysical Research: Solid Earth*, vol. 121, no. 4, pp. 2708–2726, 2016.

[26] K. W. Chang, H. Yoon, and M. J. Martinez, "Seismicity rate surge on faults after shut-in: poroelastic response to fluid injection," *Bulletin of the Seismological Society of America*, vol. 108, no. 4, pp. 1889–1904, 2018.

[27] K. W. Chang and H. Yoon, "3-D modeling of induced seismicity along multiple faults: magnitude, rate, and location in a poroelasticity system," *Journal of Geophysical Research: Solid Earth*, vol. 123, no. 11, pp. 9866–9883, 2018.

[28] P. A. Fokker, H. Hofmann, P. Meier, K.-B. Min, K. Yoon, and G. Zimmermann, "Harmonic pulse testing as a monitoring tool during hydraulic stimulation of an enhanced geothermal system," in *Proceedings, 43rd Workshop on Geothermal Reservoir Engineering*, Stanford, California, February 2018Stanford Universitypaper SGP-TR-213.

[29] A. Psyrillos, D. A. C. Manning, and S. D. Burley, "The nature and significance of illite associated with quartz-hematite hydrothermal veins in the St. Austell pluton, Cornwall, England," *Clay Minerals*, vol. 36, no. 4, pp. 585–597, 2001.

[30] K. F. Evans, A. Zappone, T. Kraft, N. Deichmann, and F. Moia, "A survey of the induced seismic responses to fluid injection in geothermal and CO_2 reservoirs in Europe," *Geothermics*, vol. 41, pp. 30–54, 2012.

[31] N. Deichmann and D. Giardini, "Earthquakes induced by the stimulation of an enhanced geothermal system below Basel (Switzerland)," *Seismological Research Letters*, vol. 80, no. 5, pp. 784–798, 2009.

[32] S. K. Chough and Y. K. Sohn, "Tectonic and sedimentary evolution of a Cretaceous continental arc–backarc system in the Korean peninsula: new view," *Earth-Science Reviews*, vol. 101, no. 3-4, pp. 225–249, 2010.

[33] S. K. Chough, S.-T. Kwon, J.-H. Ree, and D. K. Choi, "Tectonic and sedimentary evolution of the Korean peninsula: a review and new view," *Earth-Science Reviews*, vol. 52, no. 1-3, pp. 175–235, 2000.

[34] I. Metcalfe, "Palaeozoic and Mesozoic tectonic evolution and palaeogeography of East Asian crustal fragments: the Korean Peninsula in context," *Gondwana Research*, vol. 9, no. 1-2, pp. 24–46, 2006.

[35] C. W. Oh, "A new concept on tectonic correlation between Korea, China and Japan: histories from the late Proterozoic to Cretaceous," *Gondwana Research*, vol. 9, no. 1-2, pp. 47–61, 2006.

[36] T.-H. Lee, K. Yi, C.-S. Cheong, Y.-J. Jeong, N. Kim, and M.-J. Kim, "SHRIMP U-Pb zircon geochronology and geochemistry of drill cores from the Pohang Basin," *The Journal of the Petrological Society of Korea*, vol. 23, no. 3, pp. 167–185, 2014.

[37] K. Yi, C.-S. Cheong, J. Kim, N. Kim, Y.-J. Jeong, and M. Cho, "Late Paleozoic to early Mesozoic arc-related magmatism in southeastern Korea: SHRIMP zircon geochronology and geochemistry," *Lithos*, vol. 153, pp. 129–141, 2012.

[38] Y.-J. Jwa, "Mesozoic granites and associated mineralization in South Korea," in *Proceedings, the Ishihara Symposium: Granites and Associated Metallogenesis*, pp. 81–83, Sydney, Australia, July 2003.

[39] S.-G. Choi, I.-C. Ryu, S. J. Pak, S.-M. Wee, C. S. Kim, and M.-E. Park, "Cretaceous epithermal gold–silver mineralization and geodynamic environment, Korea," *Ore Geology Reviews*, vol. 26, no. 1-2, pp. 115–135, 2005.

[40] L. Jolivet and K. Tamaki, "Neogene kinematics in the Japan Sea region and volcanic activity of the Northeast Japan arc," in *Proceedings of the Ocean Drilling Program, Scientific Results*, Tamaki, K., Suyehiro, K., Allan, J., McWilliams, M., eds., vol. 127/128, pp. 1311–1331, 1992.

[41] M. Son, C. W. Song, M.-C. Kim, Y. Cheon, H. Cho, and Y. K. Sohn, "Miocene tectonic evolution of the basins and fault systems, SE Korea: dextral simple shear during the East Sea (Sea of Japan) opening," *Journal of the Geological Society, London*, vol. 172, no. 5, pp. 664–680, 2015.

[42] P.-Y. Choi, "'Singwang strike-slip duplex' around the Pohang Basin, SE Korea: its structural evolution and role in opening and fill of the Miocene basin," *Geosciences Journal*, vol. 10, no. 2, pp. 145–157, 2006.

[43] B.-H. Hwang, J.-D. Lee, K. Yang, and M. McWilliams, "Cenozoic strike-slip displacement along the Yangsan fault, southeast Korean peninsula," *International Geology Review*, vol. 49, no. 8, pp. 768–775, 2007.

[44] J. B. Kyung, "Paleoseismology of the Yangsan fault, southeastern part of the Korean peninsula," *Annals of Geophysics*, vol. 46, pp. 983–996, 2003.

[45] K. Lee and Y. Woo-Sun, "Historical seismicity of Korea," *Bulletin of the Seismological Society of America*, vol. 96, no. 3, pp. 846–855, 2006.

[46] Y. H. Kim, J. Rhie, T.-S. Kang, K.-H. Kim, M. Kim, and S.-J. Lee, "The 12 September 2016 Gyeongju earthquakes: 1. Observation and remaining questions," *Geosciences Journal*, vol. 20, no. 6, pp. 747–752, 2016.

[47] Y. Park, J.-H. Ree, and S.-H. Yoo, "Fault slip analysis of Quaternary faults in southeastern Korea," *Gondwana Research*, vol. 9, no. 1-2, pp. 118–125, 2006.

[48] H. Hofmann, G. Zimmermann, A. Zang, and K.-B. Min, "Cyclic soft stimulation (CSS): a new fluid injection protocol and traffic light system to mitigate seismic risks of hydraulic stimulation treatments," *Geothermal Energy*, vol. 6, no. 1, 2018.

[49] R. J. Pine and A. S. Batchelor, "Downward migration of shearing in jointed rock during hydraulic injections," *International Journal of Rock Mechanics and Mining Sciences & Geomechanics Abstracts*, vol. 21, no. 5, pp. 249–263, 1984.

[50] L. Xie and K.-B. Min, "Initiation and propagation of fracture shearing during hydraulic stimulation in enhanced geothermal system," *Geothermics*, vol. 59, pp. 107–120, 2016.

[51] T. C. Ekneligoda and K.-B. Min, "Determination of optimum parameters of doublet system in a horizontally fractured geothermal reservoir," *Renewable Energy*, vol. 65, pp. 152–160, 2014.

[52] Y. Lee, S. Park, J. Kim, H. C. Kim, and M.-H. Koo, "Geothermal resource assessment in Korea," *Renewable & Sustainable Energy Reviews*, vol. 14, no. 8, pp. 2392–2400, 2010.

[53] H. C. Kim and Y. Lee, "Heat flow in the Republic of Korea," *Journal of Geophysical Research*, vol. 112, no. B5, article B05413, 2007.

[54] H. S. Carslaw and J. C. Jaeger, *Conduction of Heat in Solids*, vol. 510, Clarendon Press, Oxford, 2nd ed edition, 1959.

[55] J. Lee, T.-K. Hong, and C. Chang, "Crustal stress field perturbations in the continental margin around the Korean peninsula and Japanese islands," *Tectonophysics*, vol. 718, pp. 140–149, 2017.

[56] C. Chang, J. B. Lee, and T.-S. Kang, "Interaction between regional stress state and faults: complementary analysis of borehole in situ stress and earthquake focal mechanism in southeastern Korea," *Tectonophysics*, vol. 485, no. 1-4, pp. 164–177, 2010.

[57] R. Lee, C. Chang, T.-K. Hong et al., "A comparison between deep and shallow stress fields in Korea using earthquake focal mechanism inversions and hydraulic fracturing stress measurements," *Geophysical Research Abstracts*, vol. 18, pp. EGU2016–11721-3, 2016.

[58] H. Kim, L. Xie, K.-B. Min, S. Bae, and O. Stephansson, "Integrated in situ stress estimation by hydraulic fracturing, borehole observations and numerical analysis at the EXP-1 borehole in Pohang, Korea," *Rock Mechanics and Rock Engineering*, vol. 50, no. 12, pp. 3141–3155, 2017.

[59] R. Westaway, "The importance of characterizing uncertainty in controversial geoscience applications: induced seismicity associated with hydraulic fracturing for shale gas in northwest England," *Proceedings of the Geologists' Association*, vol. 127, no. 1, pp. 1–17, 2016.

[60] J.-C. Park, W. Kim, T. W. Chung, C.-E. Baag, and J.-H. Ree, "Focal mechanisms of recent earthquakes in the southern Korean peninsula," *Geophysical Journal International*, vol. 169, no. 3, pp. 1103–1114, 2007.

[61] M. H. P. Bott, "The mechanics of oblique slip faulting," *Geological Magazine*, vol. 96, no. 2, pp. 109–117, 1959.

[62] A. Hackston and E. Rutter, "The Mohr–Coulomb criterion for intact rock strength and friction – a re-evaluation and consideration of failure under polyaxial stresses," *Solid Earth*, vol. 7, no. 2, pp. 493–508, 2016.

[63] J. Angelier, "Fault slip analysis and paleostress reconstruction," in *Continental Deformation*, P. L. Hancock, Ed., pp. 53–100, Pergamon, Oxford, 1994.

[64] N. Kato and T. Hirono, "Heterogeneity in friction strength of an active fault by incorporation of fragments of the surrounding host rock," *Earth, Planets and Space*, vol. 68, no. 1, 2016.

[65] E. M. Anderson, *The dynamics of faulting and dyke formation with applications to Britain*, Oliver and Boyd, Edinburgh, 1951.

[66] N. M. Burnside, D. Banks, and A. J. Boyce, "Sustainability of thermal energy production at the flooded mine workings of the former Caphouse Colliery, Yorkshire, United Kingdom," *International Journal of Coal Geology*, vol. 164, pp. 85–91, 2016.

[67] S.-G. Lee, T.-K. Kim, and T. J. Lee, "Strontium isotope geochemistry and its geochemical implication from hot spring waters in South Korea," *Journal of Volcanology and Geothermal Research*, vol. 208, no. 1-2, pp. 12–22, 2011.

[68] J. D. Rimstidt and H. L. Barnes, "The kinetics of silica-water reactions," *Geochimica et Cosmochimica Acta*, vol. 44, no. 11, pp. 1683–1699, 1980.

[69] S. Gudbrandsson, D. Wolff-Boenisch, S. R. Gislason, and E. H. Oelkers, "Experimental determination of plagioclase dissolution rates as a function of its composition and pH at 22 °C," *Geochimica et Cosmochimica Acta*, vol. 139, pp. 154–172, 2014.

[70] C. R. German and W. E. Seyfried, "Hydrothermal processes," in *Treatise on Geochemistry*, H. D. Holland and K. K. Turekian, Eds., pp. 191–233, Elsevier, London, 2nd ed. edition, 2014.

[71] D. L. Parkhurst and C. A. J. Appelo, *Description of input and examples for PHREEQC version 3—a computer program for speciation, batch-reaction, one-dimensional transport, and inverse geochemical calculations*, U.S. Geological Survey Techniques and Methods, Book 6, Chapter A43, 2013, May 2018, http://pubs.usgs.gov/tm/06/a43/.

[72] Y. K. Sohn, C. W. Rhee, and H. Shon, "Revised stratigraphy and reinterpretation of the Miocene Pohang basinfill, SE Korea: sequence development in response to tectonism and eustasy in a back-arc basin margin," *Sedimentary Geology*, vol. 143, no. 3-4, pp. 265–285, 2001.

[73] S.-G. Lee, T.-K. Kim, J.-S. Lee, T. J. Lee, B. W. Cho, and H. J. Koh, "Geochemical implication of $^{87}Sr/^{86}Sr$ ratio of high-temperature deep groundwater in a fractured granite aquifer," *Geochemical Journal*, vol. 42, no. 5, pp. 429–441, 2008.

[74] H. Yasuhara, C. Marone, and D. Elsworth, "Fault zone restrengthening and frictional healing: the role of pressure solution," *Journal of Geophysical Research*, vol. 110, no. B6, article B06310, 2005.

[75] S. A. Miller, "The role of fluids in tectonic and earthquake processes," *Advances in Geophysics*, vol. 54, pp. 1–46, 2013.

[76] V. I. Keilis-Borok, "On estimation of the displacement in an earthquake source and of source dimensions," *Annali di Geofisica*, vol. 12, pp. 205–214, 1959.

[77] T. C. Hanks and H. Kanamori, "A moment magnitude scale," *Journal of Geophysical Research*, vol. 84, no. B5, pp. 2348–2350, 1979.

[78] S. Ide and G. C. Beroza, "Does apparent stress vary with earthquake size?," *Geophysical Research Letters*, vol. 28, no. 17, pp. 3349–3352, 2001.

[79] B. E. Shaw, "Constant stress drop from small to great earthquakes in magnitude-area scaling," *Bulletin of the Seismological Society of America*, vol. 99, no. 2A, pp. 871–875, 2009.

[80] J. F. Archard, "Elastic deformation and the laws of friction," *Proceedings of the Royal Society of London. Series A. Mathematical and Physical Sciences*, vol. 243, no. 1233, pp. 190–205, 1957.

[81] E. K. Mitchell, Y. Fialko, and K. M. Brown, "Temperature dependence of frictional healing of Westerly granite: experimental observations and numerical simulations," *Geochemistry, Geophysics, Geosystems*, vol. 14, no. 3, pp. 567–582, 2013.

[82] C. A. Barton, M. D. Zoback, and D. Moos, "Fluid flow along potentially active faults in crystalline rock," *Geology*, vol. 23, no. 8, pp. 683–686, 1995.

[83] J. Townend and M. D. Zoback, "How faulting keeps the crust strong," *Geology*, vol. 28, no. 5, p. 399, 2000.

[84] M. L. Zoback and M. D. Zoback, "Lithosphere stress and deformation," in *Treatise on Geophysics*, vol. 6, pp. 253–273, 2007.

[85] W. F. Brace and D. L. Kohlstedt, "Limits on lithospheric stress imposed by laboratory experiments," *Journal of Geophysical Research*, vol. 85, no. B11, pp. 6248–6252, 1980.

[86] F. M. Chester and J. M. Logan, "Composite planar fabric of gouge from the Punchbowl fault, California," *Journal of Structural Geology*, vol. 9, no. 5-6, pp. 621–IN6, 1987.

[87] J. S. Caine, J. P. Evans, and C. B. Forster, "Fault zone architecture and permeability structure," *Geology*, vol. 24, no. 11, pp. 1025–1028, 1996.

[88] J.-H. Choi, P. Edwards, K. Ko, and Y.-S. Kim, "Definition and classification of fault damage zones: a review and a new methodological approach," *Earth-Science Reviews*, vol. 152, pp. 70–87, 2016.

[89] D. R. Faulkner, A. C. Lewis, and E. H. Rutter, "On the internal structure and mechanics of large strike-slip fault zones: field observations of the Carboneras fault in southeastern Spain," *Tectonophysics*, vol. 367, no. 3-4, pp. 235–251, 2003.

[90] Z. K. Shipton and P. A. Cowie, "A conceptual model for the origin of fault damage zone structures in high-porosity sandstone," *Journal of Structural Geology*, vol. 25, no. 3, pp. 333–344, 2003.

[91] Y.-S. Kim, D. C. P. Peacock, and D. J. Sanderson, "Fault damage zones," *Journal of Structural Geology*, vol. 26, no. 3, pp. 503–517, 2004.

[92] S. J. Martel and W. A. Boger, "Geometry and mechanics of secondary fracturing around small three-dimensional faults in granitic rock," *Journal of Geophysical Research*, vol. 103, no. B9, pp. 21299–21314, 1998.

[93] B. K. Kim, "Cenozoic biostratigraphy of South Korea," *Palaeogeography, Palaeoclimatology, Palaeoecology*, vol. 46, no. 1-3, pp. 85–96, 1984.

[94] H. S. Lim, Y. I. Lee, and K. D. Min, "Thermal history of the Cretaceous Sindong Group, Gyeongsang Basin, Korea, based on fission track analysis," *Basin Research*, vol. 15, no. 1, pp. 139–152, 2003.

[95] US Geological Survey 2018, *M 5.5 - 7km WSW of Heung-hai, South Korea. U.S. Geological Survey Earthquake Hazards Program*, US Geological Survey, Reston, Virginia, 2018, https://earthquake.usgs.gov/earthquakes/eventpage/us2000bnrsmoment-tensor.

[96] C.-M. Kim, R. Han, G. Y. Jeong, J. O. Jeong, and M. Son, "Internal structure and materials of the Yangsan fault, Bogyeongsa area, Pohang, South Korea," *Geosciences Journal*, vol. 20, no. 6, pp. 759–773, 2016.

[97] Gyeongsangbuk-do Tour 2016, *Pohang hot spring*, Gyeongsangbuk-do Tourist Information, Andong, Korea, 2018, http://tour.gb.go.kr/en/page.do?con_uid=20098&cmd=2&mnu_uid=298.

[98] K. C. Devkota, J.-E. Ham, and G.-W. Kim, "Characteristics of discontinuity spacing of Yeongdeok granite," *Geosciences Journal*, vol. 13, no. 2, pp. 161–165, 2009.

[99] P. L. Hancock and T. Engelder, "Neotectonic joints," *Geological Society of America Bulletin*, vol. 101, no. 10, pp. 1197–1208, 1989.

[100] R. J. H. Jolly and D. J. Sanderson, "A Mohr circle construction for the opening of a pre-existing fracture," *Journal of Structural Geology*, vol. 19, no. 6, pp. 887–892, 1997.

[101] J. F. Labuz and A. Zang, "Mohr–Coulomb failure criterion," *Rock Mechanics and Rock Engineering*, vol. 45, no. 6, pp. 975–979, 2012.

[102] Lenntech 2018, *Major Ion Composition of Seawater*, Lenntech Water Treatment Solutions BV, Delft, The Netherlands, 2018, https://www.lenntech.com/composition-seawater.htm.

[103] Stanford University 2018, *Mineral makeup of seawater*, Stanford University, Stanford, California, 2018, https://web.stanford.edu/group/Urchin/mineral.html.